NEUROTECHNOLOGY

Constructing 2D maps of human spinal cord activity and isolating the functional midline with high-density microelectrode arrays

Samantha M. Russman[1,2], Daniel R. Cleary[2,3], Youngbin Tchoe[2], Andrew M. Bourhis[2], Brittany Stedelin[4], Joel Martin[2,3], Erik C. Brown[4], Xinlian Zhang[5], Aaron Kawamoto[4], Won Hyung A. Ryu[4], Ahmed M. Raslan[4], Joseph D. Ciacci[3], Shadi A. Dayeh[1,2]*

Intraoperative neuromonitoring (IONM) is a widely used practice in spine surgery for early detection and minimization of neurological injury. IONM is most commonly conducted by indirectly recording motor and somatosensory evoked potentials from either muscles or the scalp, which requires large-amplitude electrical stimulation and provides limited spatiotemporal information. IONM may inform of inadvertent events during neurosurgery after they occur, but it does not guide safe surgical procedures when the anatomy of the diseased spinal cord is distorted. To overcome these limitations and to increase our understanding of human spinal cord neurophysiology, we applied a microelectrode array with hundreds of channels to the exposed spinal cord during surgery and resolved spatiotemporal dynamics with high definition. We used this method to construct two-dimensional maps of responsive channels and define with submillimeter precision the electrophysiological midline of the spinal cord. The high sensitivity of our microelectrode array allowed us to record both epidural and subdural responses at stimulation currents that are well below those used clinically and to resolve postoperative evoked potentials when IONM could not. Together, these advances highlight the potential of our microelectrode arrays to capture previously unexplored spinal cord neural activity and its spatiotemporal dynamics at high resolution, offering better electrophysiological markers that can transform IONM.

INTRODUCTION

Spinal surgeries most often work around the spinal cord, nerve roots, and associated blood vessels, with some cases requiring entry into the neural elements. In either case, surgery has an inherent risk for debilitating or devastating postoperative neurological deficits (*1*–*4*). For surgery involving the spinal cord and nerves, this risk is particularly profound when a safe entry or dissection pathway cannot be readily identified, such as when resecting intradural spinal cord tumors (*5*). For surgeries with risk of neurological injury, the surgeons will often use intraoperative neuromonitoring (IONM) of the spinal cord to indirectly assess the functional integrity of motor and sensory pathways when operating in or around spinal neural structures.

IONM has previously been shown to improve surgical outcomes (*1*–*4*, *6*–*10*), but in its current form, it only provides an indirect evaluation of the structural and functional spinal pathways. During IONM, somatosensory evoked potentials (SSEPs) are recorded from the scalp in response to electrical current stimulation of a peripheral nerve, and motor evoked potentials (MEPs) (*11*–*15*) are recorded from the upper and lower limb muscles in response to transcranial electrical stimulation (*16*–*19*). In recording SSEPs from the brain, the scalp, cranium, and dura all act as insulators, resulting in low-amplitude responses. As a result, high-amplitude stimulation currents must be applied with high-count stimulation trains to improve signal-to-noise ratio (SNR) of the averaged recordings and extract electrophysiological signals from the recording system's baseline noise (*19*–*21*). These stimulation trains also prevent real-time monitoring, where neurological injuries may not be noticeable for many minutes after the triggering event (*22*). Last, the physical separation of the recording contacts on the scalp from the surgical site on the spinal cord prevents recording of spatiotemporal, anatomical, and physiological features of responses.

IONM is also not without controversies. The sensitivity and specificity of SSEP and MEP are not perfect, where false positives may lead to cessation of surgery and incomplete resection and false negatives may lead to undetected injury (*23*–*25*). In addition, there is still the practice of wake-up testing in certain spine surgeries such as scoliosis. Moreover, SSEPs may not change if the injury is purely motor or vascular.

We hypothesized that direct recording of SSEPs by microelectrodes on the surface of the spinal cord could increase the fidelity of these recordings and reduce the number of required trials, allowing real-time spatiotemporal mapping. We also predicted that recordings with a high– channel count microelectrode array would offer two-dimensional (2D) SSEP responses, which would allow for more precise identification of the spinal cord functional midline at the point of resection. The functional midline is the only safe corridor to the inner structure of the spinal cord; therefore, its identification is of critical relevance. Unfortunately, there is no consistent or accurate anatomic landmark to the midline on the surface; moreover, it is often distorted with tumors/masses or rotated because of adhesions. Precise functional midline identification would be advantageous given that the position of the anatomical and functional midline has been found to be mismatched by up to 2 mm in 40% of patients (*26*, *27*). Dorsal column (DC) mapping in spinal cord surgery was shown to decrease the occurrence of new postoperative sensorimotor dysfunction by 42% (*28*). There are limited studies

[1]Department of Bioengineering, University of California, San Diego, La Jolla, CA 92093, USA. [2]Integrated Electronics and Biointerfaces Laboratory, Department of Electrical and Computer Engineering, University of California, San Diego, La Jolla, CA 92093, USA. [3]Department of Neurosurgery, University of California, San Diego, La Jolla, CA 92093, USA. [4]Department of Neurosurgery, Oregon Health & Science University, Portland, OR 97239, USA. [5]Division of Biostatistics and Bioinformatics, Herbert Wertheim School of Public Health, University of California, San Diego, La Jolla, CA 92093, USA.
*Corresponding author. Email: sdayeh@eng.ucsd.edu

that reported DC mapping by recording SSEPs directly from the surface of the spinal cord using linear eight-contact arrays (*29*, *30*). In these studies, sparse mapping of the midline was performed by direct electrical stimulation of the DC using a linear array of eight contacts made of Teflon-coated stainless steel wires that were 76 μm in diameter and 1 mm apart. The midline was identified by phase reversal in the recorded SSEPs. In two other studies, SSEPs were stimulated from the spinal cord surface and recorded from the brain, again identifying a rudimentary functional midline (*31*, *32*).

We fabricated high–channel number microelectrode arrays by leveraging low-impedance contact materials that we have used before in cortical recordings such as poly(3,4-ethylenedioxythiophene) polystyrene sulfonate (PEDOT:PSS) (*33*–*36*) and platinum nanorod (PtNR) (*37*) contacts. Our electrodes were fabricated on thin (~6.6-μm) parylene C substrates (*38*, *39*), which allowed for high conformability to the pial surface of the spinal cord during IONM. We observed dynamic patterns of ipsilateral and contralateral SSEPs with high resolution that allowed us to identify a microscale midline boundary. This high-resolution boundary was identified at clinical stimulation currents and persisted even when scalp SSEPs could not be identified. Our microelectrode array also outperformed clinical equipment given that our recordings were directly on the spinal cord surface and thus did not require substantial trial averaging. In the future, this technology could provide a practically instantaneous IONM method once data analysis and plotting are incorporated in real time. Together, our microelectrode grid can improve IONM and could have other applications, such as for evaluation or even treatment of spinal cord injury (SCI).

RESULTS

Experiment design and surgical implantation

To assess the viability of recording spatiotemporal SSEP patterns with high quality and resolution from the surface of the spinal cord, we recorded SSEPs with a high-density microelectrode array in individuals (n = 6) undergoing intramedullary tumor or biopsy procedures in the cervical spinal cord (Fig. 1A). The microelectrode array recordings were adjunct to the surgery, completed with minimal disruption to the surgical flow of the procedure time, and performed with Institutional Review Board (IRB) authorization at the University of California, San Diego (UCSD) and at Oregon Health & Sciences University (OHSU). The microelectrode array recordings were performed during three time points in the surgery: epidurally and subdurally before tumor resection or biopsy and subdurally after resection or biopsy. The electrode was placed on the exposed surface spinal cord for tumor resection, covered the DCs, and was centered over the anatomical midline of the spinal cord. That surface placement spanned an apparently normal area of the spinal cord rostral and caudal to the lesion. The placement was documented with intraoperative photos from the surgical microscope. Suction and sponges were used to remove excess blood and cerebrospinal fluid from the spinal cord surface to ensure good electrode-tissue contact during the recordings (Fig. 1B). Suction and sponges near the electrode did not negatively affect recording quality or introduce substantiative noise into the data.

Electrode design

Multiple-electrode designs were used in the recordings from the six participants (table S1), with results presented in this work from participants 4 to 6. Recordings from these participants used a single-electrode design and leveraged a long, high-density connector that was not available for the earlier participants (Fig. 1C). In addition, the overall width of the electrode was reduced from 1.6 cm to 6.4 mm in the final design to maintain stable contact with the DC and account for variable width of the surgical area. These participants

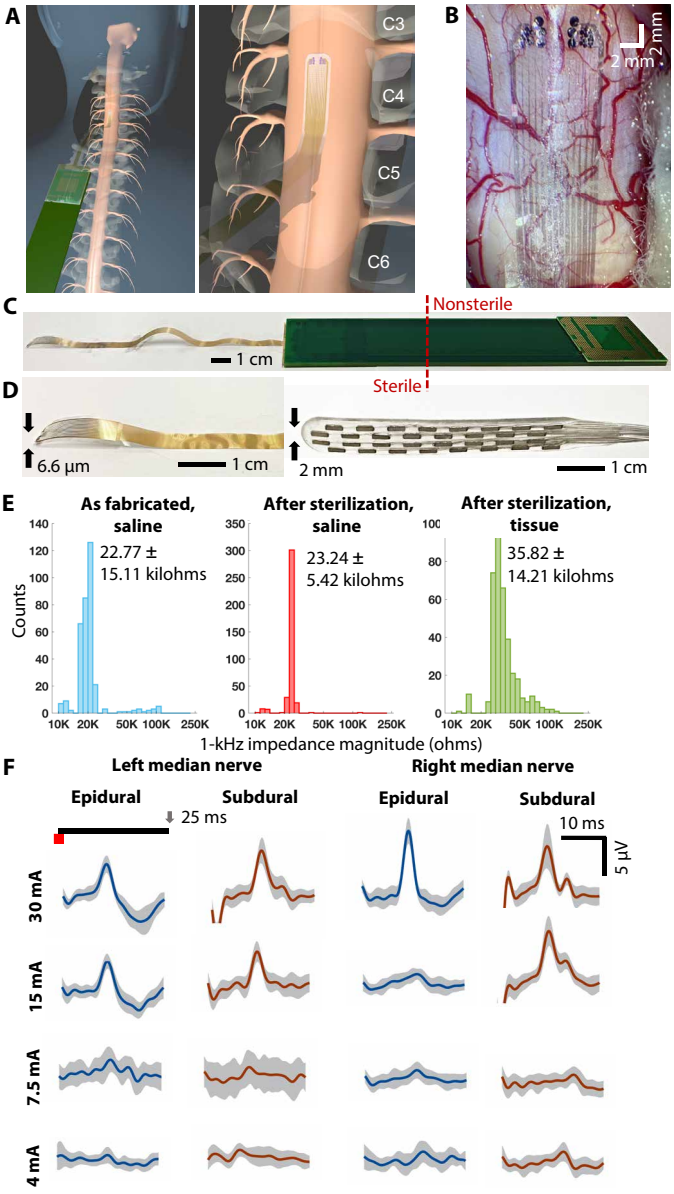

Fig. 1. Experiment overview and electrode design. (**A**) Schematic diagram of the placement of the research grid on the participant's spinal cord. (**B**) Photograph of the research grid placed on the subdural surface of spinal cord during recording. (**C**) Research microelectrode bonded to extender PCB with the sterile/nonsterile junction point highlighted. (**D**) Comparison of size and thickness of the research microelectrode versus a clinical grid (CoverEdge X 32, Boston Scientific). (**E**) One-kilohertz impedance magnitude histograms measured as fabricated in saline, after sterilization in saline, and on spinal cord tissue. (**F**) Example single-channel responses to different left and right median nerve stimulation current amplitudes recorded epidurally and subdurally before resection. The channel with the highest peak-to-peak amplitude response was chosen as the example channel for each condition.

were temporarily implanted with a microelectrode array with 372 PtNR contacts (diameter, 30 μm) arranged in a rectangular array of 12 × 31 with 350-μm horizontal (circumferential) pitch and 400-μm vertical (axial) pitch, providing a coverage area of 3.85 mm by 12 mm. At the tip of the array, an additional 54 contacts of variable diameter in the range of 30 to 480 μm were arranged in clusters of three contacts per diameter on the left and right sides of the array. The goal of the multidiameter array was to validate the effectiveness of small contact sizes in recording high-quality SSEPs.

The electrodes were designed to have a sterile/nonsterile interface junction along a long connector board (Fig. 1C) to facilitate the use of these devices in the operating room (OR). Whereas the whole thin-film device and extender board of Fig. 1C were sterilized at the hospital before use, the extender board separated the recording electronics board from the sterile area, allowing it to be encased in a sterile bag, thus maintaining an overall sterile field in the OR. Additional details on packaging, sterilization, and OR use have been previously reported (*40*).

Our 6.6-μm parylene C microelectrode arrays were much thinner than current clinical spinal cord grids (1-mm-thick silicone; Fig. 1D), therefore more conformal to the spinal surface and compliant to movement during recording. In addition, the microelectrode arrays were transparent, which gave the surgeon an unobstructed view of the surface spinal anatomical features when the grid was in place. The 1-kHz electrochemical impedance of the microelectrode array used in participant 5 measured in phosphate-buffered saline after fabrication was 22.77 ± 15.11 kilohms. The impedance values did not change significantly ($P = 0.5926$) after Sterrad sterilization, a hydrogen peroxide gas plasma technology that is compatible with the PtNRGrids (*40*), and were 23.24 ± 5.42 kilohms after sterilization (Fig. 1E). On the pial surface, the contacts exhibited slightly higher impedance values, with a mean of 35.82 ± 14.21 kilohms, an increase that is expected when measuring on tissue (*41*). These impedance values are representative of those measured across participants 4 to 6 (fig. S1). Our recording analysis focused on microelectrode contacts that exhibited a 1-kHz impedance lower than 120 kilohms because recordings with contacts with higher impedances are susceptible to noise. After fabrication, sterilization, and throughout multiple surgical placements and recordings, our microelectrode arrays maintained a yield above 87% (Fig. 1E and fig. S1). These measurements show the stability of the microelectrode array throughout sterilization and all experimental procedures.

Stimulation paradigm

The IONM team delivered electrical stimulation to both upper limb (typically median) and lower limb (typically tibial) nerves in trains of 40 at 2.78 Hz. Stimulation current amplitudes were initially set to clinical amplitudes used by the IONM team between 30 and 50 mA depending on the participant. The stimulation amplitudes were then decreased to one-half, one-fourth, and one-eighth of these clinical amplitudes. For participant 5, the current amplitudes used were therefore 30, 15, 7.5, and 4 mA, the last of which was the lowest current amplitudes used for stimulation across all patients.

Response amplitudes and thresholds

For both epidural and subdural placements, SSEPs had an onset latency of 10 ms and a peak latency of ~12 ms (Figs. 1F and 2, A to D). This is consistent with previous recordings with low–channel count microgrids from the surface of the spine (*11*, *42*, *43*). Averaged maximal peak-to-peak SSEP amplitudes ranged from 8 to 10 μV for 30-mA stimulation to ~1 μV for 4-mA stimulation for 30 to 40 trials. Representative channels with high response amplitudes are shown in Fig. 1F. Statistical analysis was used to evaluate whether the peak-to-peak amplitudes were statistically significant compared to prestimulus baseline. This was particularly a question for low stimulation currents where the SNR was low, which we classified as below SNR = 6 (Table 1). A Mann-Whitney *U* test showed significance at almost all current amplitudes at $P < 0.001$ (Table 1). However, for 4-mA current amplitudes in both epidural and subdural placements, the effect size was equal to or less than 1, indicating that any differences may not be observable or clinically relevant. A similar low effect size of −1.15 was observed for 15-mA left subdural recording, which we suspect was caused by a fluid buildup on the spinal cord, leading to poor electrode-tissue contact for this stimulation amplitude. In general, for high current amplitudes, response amplitudes were significant (*P* values can be found in Table 1) for both epidural and subdural placements. Overall, these results indicate that both placements are appropriate for detection of neural signals.

During each case, we also performed a control recording on skin to confirm that the changes in voltage that we observed were due to neural activity and not the stimulation artifact. In this participant, the peak-to-peak amplitudes of skin recordings at the clinical stimulation amplitude were below 1 μV (mean, 0.56 ± 0.18 μV), which was lower compared to the baseline (mean, 0.75 ± 0.24 μV) (fig. S2). Similar patterns were observed among all participants (data file S1).

Spatiotemporal response patterns

Our microelectrode array was placed on the spinal cord, allowing it to capture spatiotemporal features of the SSEPs, which current IONM clinical equipment cannot resolve because the recording electrodes are placed on the surface of the scalp. Whereas amplitudes of the responses were similar between the epidural and subdural placements, subdural recordings were more localized, especially for higher current amplitudes where response amplitude varied substantially across the array (Fig. 2, A to D). Epidural recordings showed more uniform responses across channels compared to subdural recordings, which manifested in a wider spread of responses across the array. Spatiotemporal profiles of subdural recordings showed similar patterns in response propagation for different stimulation currents. A plot of peak-to-peak responses for all current amplitudes calculated from these time evolution plots is shown in fig. S3. These response patterns and dependencies on stimulation currents are consistent with recordings from other participants (figs. S4 and S5). Higher response amplitudes were registered on the side of the body where the stimulation was delivered; left channels were more responsive for left median nerve stimulation and right channels for right median nerve stimulation. This is consistent with spinal cord anatomy because the DCs are largely ipsilateral to the peripheral nerves entering the spine.

The conduction velocity of the SSEPs was calculated from the approximate distance of the median nerve stimulating electrode to the recording microelectrode and the peak latency. This was found to be 50 ± 4.5 m/s, assuming an arm length of 0.6 m. Previous reports provide conduction velocities in the range of 91.3 ± 7.2 m/s for Aα nerve fibers (*44*) and 63.4 ± 4.5 m/s (*45*) and 69.3 ± 6.6 m/s for Aβ nerve fibers, which carry sensory information (*46*). Our lower estimated conduction velocity might be explained by errors in estimation of arm length and the synapsing of the nerve fibers

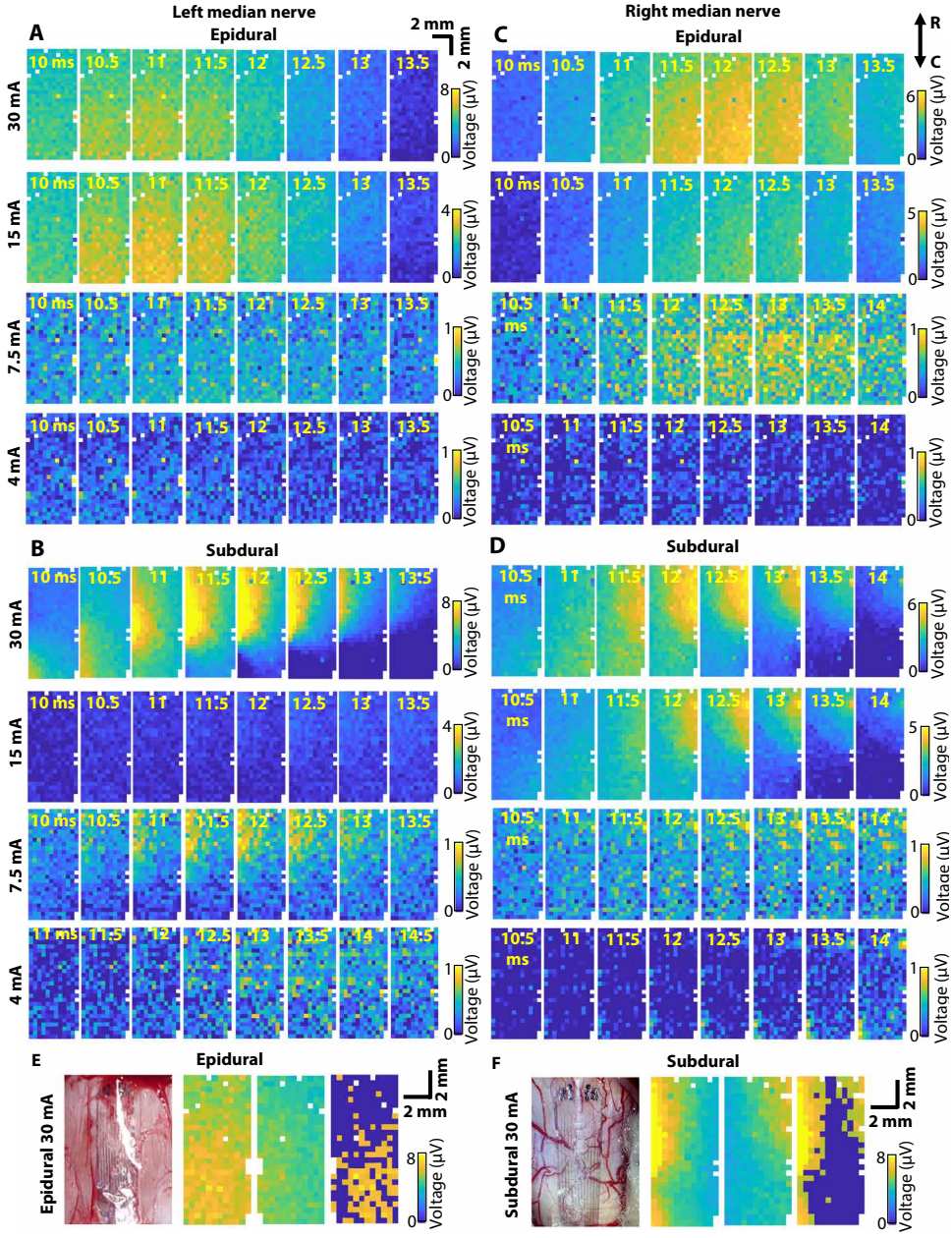

Fig. 2. Time evolution plots of recorded SSEPs and functional midline mapping. (**A** to **D**) Spatial distribution of peak-to-peak amplitudes of responses to both left and right median nerve stimulation recorded epidurally and subdurally before resection. Rostral (R) and caudal (C) directions are defined at top. (**E**) Functional midline estimation from epidural recording of responses to 30-mA left and right median nerve stimulation. (**F**) Functional midline estimation from subdural recording of responses to 30-mA left and right median nerve stimulation. Peak-to-peak response amplitudes over the entire recording segment can be found in fig. S3.

onto interneurons in the spinal cord. Our calculated SSEP and the onset time of the response could be used to assess neurological damage because changes over 10% in onset latency in clinically recorded scalp SSEPs are considered a sign of spinal cord dysfunction (*47*).

Mapping of the functional midline

The anatomical spinal cord midline in normal tissue can be identified anatomically by the dorsal median sulcal vein as it enters the midline raphe or at the middle point between the root entry zones on either side of the cord (*29*). This anatomical midline can be distorted by tumors, edema, neovascularization, or scar formation, prohibiting its identification using anatomical landmarks. To prevent inadvertent dissection of the DCs, which can result in postoperative morbidity that can be disabling, functional mapping is used to locate the midline to inform the spinal incisions (myelotomy). Using the spatiotemporal features of the recorded SSEPs, we performed analysis to map the functional midline for epidural and subdural recordings before resection and subdural recordings after resection. The midline was identified with better precision in the subdural recording, which is consistent with the more localized response profiles for this placement. By tuning the thresholding method for positive responses and their amplitudes as described in Materials and Methods, we were able to isolate ipsilateral responses to stimulation and outline a midline spanning two to five channels equivalent to a distance of 700 μm to 1.75 mm (Fig. 2F). This mapping is of higher resolution than reported previously with the use of eight-channel microgrids (*29*, *30*), where their contact spacing was equal to or larger than 1 mm. In addition, with our microelectrode, the midline can be traced in the rostrocaudal direction, which cannot be done with the linear microgrid. The epidural functional midline was difficult to define, given the large spread of the responses (Fig. 2E). These results were consistent in participant 4 (fig. S6). We were not able to identify the midline in patient 6, given the positioning of the electrode and tumor effects (fig. S7). Subdural postresection placement also allowed for identification of the functional midline, which is described in a later section. These results show that subdural placement allows mapping of the functional midline.

Spatial phase gradient analysis of response propagation

We performed an analysis of the spatial phase gradient of the response to better understand response propagation. We calculated the phase gradients and overlaid streamlines for better visualization of wave propagation dynamics. We hypothesized that the neural responses originate from a bundle of axons deep within the spinal cord, and therefore, we would expect to see the electric field lines aligned parallel to the axons generating action potentials, dropping off in strength radially from the center of these axons (*48*). The

Table 1. Statistical analysis and significance of results from participant 5.

	Mean SNR	*T* test	Effect size
Epidural left			
30 mA	26.79 ± 0.93	2.45×10^{-119}	−1.73
15 mA	19.49 ± 1.29	2.45×10^{-119}	−1.73
7.5 mA	8.53 ± 2.05	1.24×10^{-112}	−1.67
4 mA	1.19 ± 0.12	4.32×10^{-17}	0.73
Epidural right			
30 mA	14.25 ± 0.46	2.45×10^{-119}	−1.73
15 mA	18.94 ± 1.66	6.89×10^{-119}	−1.73
7.5 mA	5.11 ± 0.76	8.27×10^{-78}	−1.39
4 mA	3.00 ± 0.69	4.60×10^{-5}	0.29
Subdural left			
30 mA	28.86 ± 2.27	7.50×10^{-25}	−1.72
15 mA	5.62 ± 1.02	7.45×10^{-12}	−1.15
7.5 mA	8.24 ± 1.71	2.53×10^{-20}	−1.54
4 mA	3.67 ± 0.82	0.0145	−1.00
Subdural right			
30 mA	9.08 ± 0.45	7.50×10^{-25}	−1.72
15 mA	17.62 ± 3.15	5.29×10^{-23}	−1.79
7.5 mA	4.47 ± 1.05	0.275	−0.14
4 mA	4.69 ± 1.42	4.19×10^{-4}	−0.64

microelectrode array captures the 2D projection of these electric field lines along the surface of the spinal cord. Furthermore, because the neural response is propagating vertically in a rostral direction, the electric field strength will also vary as a function of time. Thus, the spatial phase gradient should primarily point in the direction of the traveling action potentials, although, because of the complex nature of the 2D projected electric field lines, it will also spread outward from the center of the response in the direction of decreasing electric field strength. We observed these phase gradient features in the subdural preresection and, to a lesser extent, in the postresection recordings (Fig. 3). Postresection recordings will be discussed below. We did not see a strong directionality of the phase gradient in the epidural recordings, which can be explained by the wide spread of potential across the array, resulting in small changes in phase. Videos of the time evolution of the response, phase gradients, and streamlines are shown (movies S1 to S6). Phase gradient plots provide another means for SSEP monitoring and may inform of changes in SSEP propagation during surgical resection.

Validation of high-quality recordings with smaller PtNR contacts

Our microelectrode array included a multidiameter array at the tip to investigate any diameter dependency of the recorded SSEPs and to confirm that smaller contact diameters, necessary for high-resolution mapping, do not lead to loss of information that is otherwise captured by larger contact diameter arrays. Larger contact diameters may have higher probability to overlap with fibers responsive to stimulation and may therefore potentially produce higher amplitude responses at lower stimulation currents. The diameters included were 30, 60, 80, 110, 140, 170, 210, 240, and 480 μm. The contacts were organized in two mirrored clusters of three contacts per diameter (Fig. 4, A and B). Peak-to-peak amplitude responses from the left- and right-side clusters showed stronger variation in the subdural versus epidural placement (Fig. 4C), with contacts positioned ipsilaterally to the stimulation side showing a stronger response compared to contacts positioned contralaterally. For example, epidural 30-mA left median nerve stimulation resulted in the 140-μm left cluster recording an amplitude of 4.85 ± 0.09 μV versus the right cluster recording an amplitude of 5.07 ± 0.06 μV. Subdurally, those left and right clusters recorded amplitudes of 7.26 ± 0.06 μV and 4.09 ± 0.15 μV, respectively (Fig. 4D). Given that there was strong spatial variability across the array and the variable diameter electrodes were inherently in different locations, we could not directly compare the peak-to-peak amplitude responses. Therefore, we also evaluated the prestimulus baseline SD for the contacts, with the assumption that this parameter should not be affected by the contact position. We found that the baseline SD did not show a conclusive diameter dependency in either the epidural or subdural placement (Fig. 4, E and F). Epidural baseline SD was consistently ~0.38 μV, whereas subdural baseline SD was ~0.18 μV. Last, we computed the power spectral density (PSD) for both the epidural and subdural recordings over a 300-ms time segment after stimulus (Fig. 4, G and H). We did not see a diameter effect on the PSD, with all channels exhibiting a 1/*f* noise relationship followed by white noise. These data suggest that recording with 30-μm-diameter PtNR contacts is as effective as recording with larger diameters, which further substantiates their use for high-definition mapping from the surface of the spinal cord.

Comparison to clinical IONM recordings

In participants 5 and 6, we sought to understand how the research microelectrode recordings compared to clinical IONM recordings. Recordings from the microelectrode array could not be directly compared to those from the IONM equipment given the difference in trial numbers used to obtain the averaged traces for both. Only 30 to 40 trials were used in the averaging for the research grid at each current amplitude. The clinical IONM recordings needed longer stimulation trains, given the lower amplitudes of responses at the scalp. As a result, the length of recording data segment that was averaged to achieve the mean traces differed between the research grid and clinical IONM data. However, a comparison could be made on the basis of the general timeline of the surgery because any substantial changes in SSEPs were noted in the log sheet and typically lasted throughout the entire experiment recording session.

Epidural and subdural preresection and subdural postresection recordings at 30 mA were compared to IONM recordings from similar time points in the surgery (Fig. 5). Research grid recordings showed a higher response amplitude compared to IONM recordings. For high current amplitudes, the range of response amplitudes measured with the research grid was much higher than for clinical IONM recordings, where 30-mA right median nerve stimulation resulted in a maximal 3-μV peak-to-peak amplitude response for the clinically recorded C3-C4 trace compared to microelectrode recordings of >8- and >6-μV responses for the 30-mA left and right stimulation, respectively (Fig. 5, A and B). The remaining clinical traces were only ~1 μV.

Although there was a loss of response to median nerve stimulation after resection in participant 5, affecting the right side more

strongly, our microelectrodes still resolved responses; however, these responses were smaller than the preresection amplitudes. The maximum response amplitude decreased from 10 to 2.5 μV, whereas the clinical IONM equipment could not register a response (Fig. 5, C and D). Furthermore, the spatial variation in the responses was preserved in the microelectrode recordings. Stimulation with 30 mA resulted in clear left and right activation patterns, similar to those seen before resection (Fig. 5, E and F). The ability to map the functional midline was also preserved (Fig. 5G). Similarly, in participant 6, the research microelectrode recordings were of higher amplitude compared to the clinical recordings throughout the surgery (fig. S8). These results highlight the potential of our microelectrode grids for IONM.

DISCUSSION

Currently deployed clinical spinal cord arrays are limited in usability by size. The thickness of these electrodes is at least on the scale of tens or hundreds of micrometers and often much thicker (*29*–*32*, *49*). As a result, these electrodes have poor contact with the spinal cord and record lower amplitude responses, requiring higher stimulation currents. Moreover, existing clinical microelectrodes typically have platinum contacts. Platinum has high impedance, requiring large contact diameters and resulting in low-resolution coverage. Large diameters limit the number of contacts across the circumference of the spinal cord, encumbering the isolation of the midline. The microelectrode arrays that we developed address these limitations and could therefore be used for high-resolution functional mapping of the spinal cord. Because our grids are fabricated on parylene, they can be much thinner (here, 6.6 μm thick) than platinum electrodes. Electrode contacts are composed of PtNRs and have much lower impedances compared to standard planar platinum contacts. The lower impedance of PtNRs enables scaling of the contact diameter while preserving excellent impedance values (~36 kilohms at 30-μm diameter) and recording capabilities, which offers the possibility of having higher density coverage.

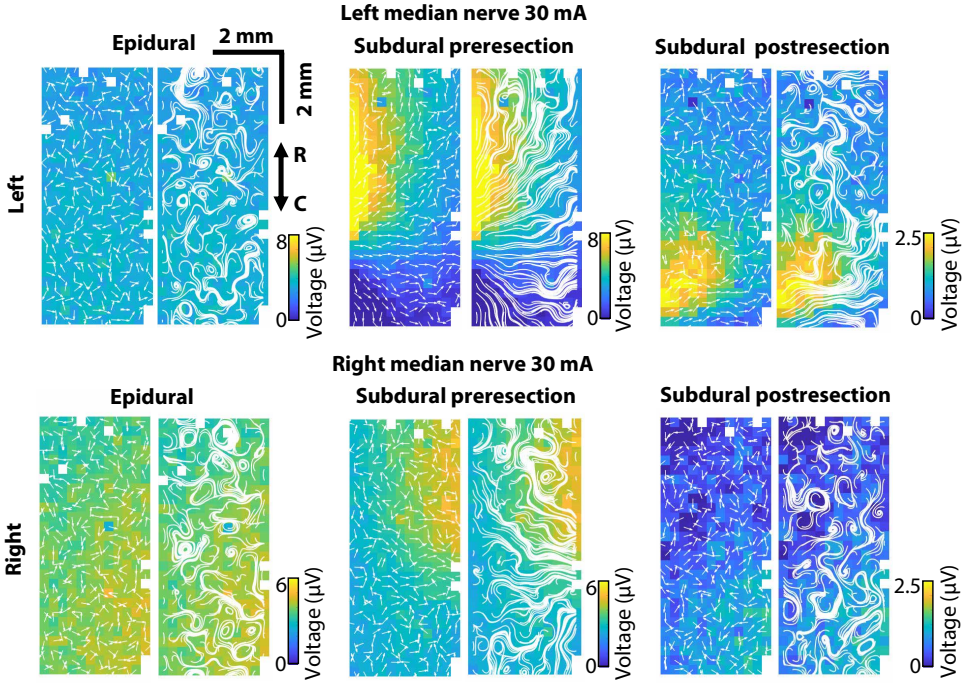

Fig. 3. Spatial phase gradients and streamlines of SSEP responses. SSEP spatial phase gradients and streamlines in response to 30-mA left (top) and right (bottom) median nerve stimulation.

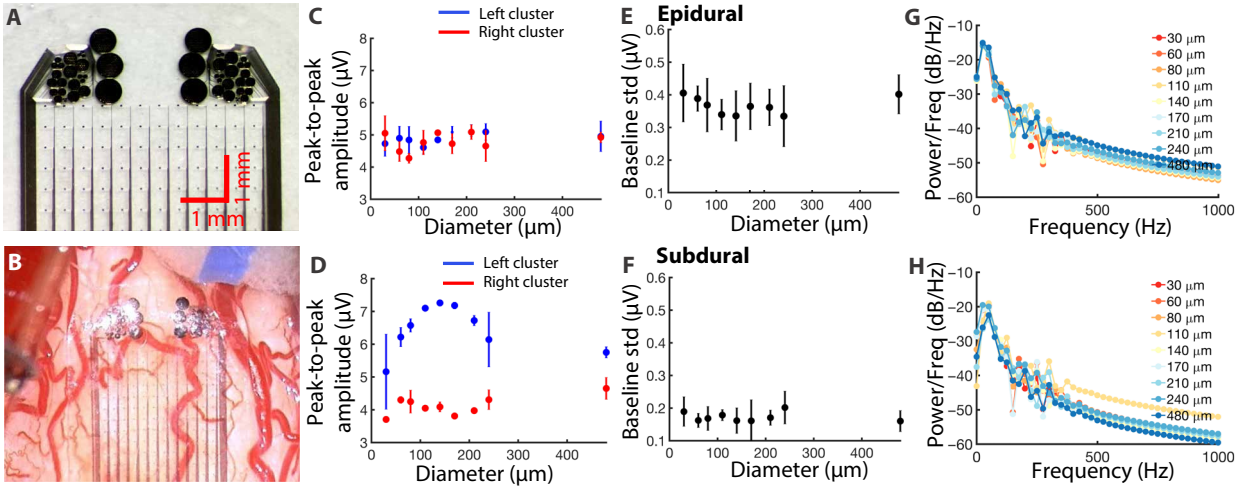

Fig. 4. Multidiameter array response analysis. (**A**) Image of multidiameter array at tip of research microelectrode. (**B**) Image of electrode placed subdurally on spinal cord during recording. (**C** and **D**) Averaged peak-to-peak amplitude responses recorded epidurally and subdurally to 30-mA left median nerve stimulation. (**E** and **F**) Averaged baseline SD recorded epidurally and subdurally. (**G** and **H**) PSD analysis on baseline recordings from (E) and (F).

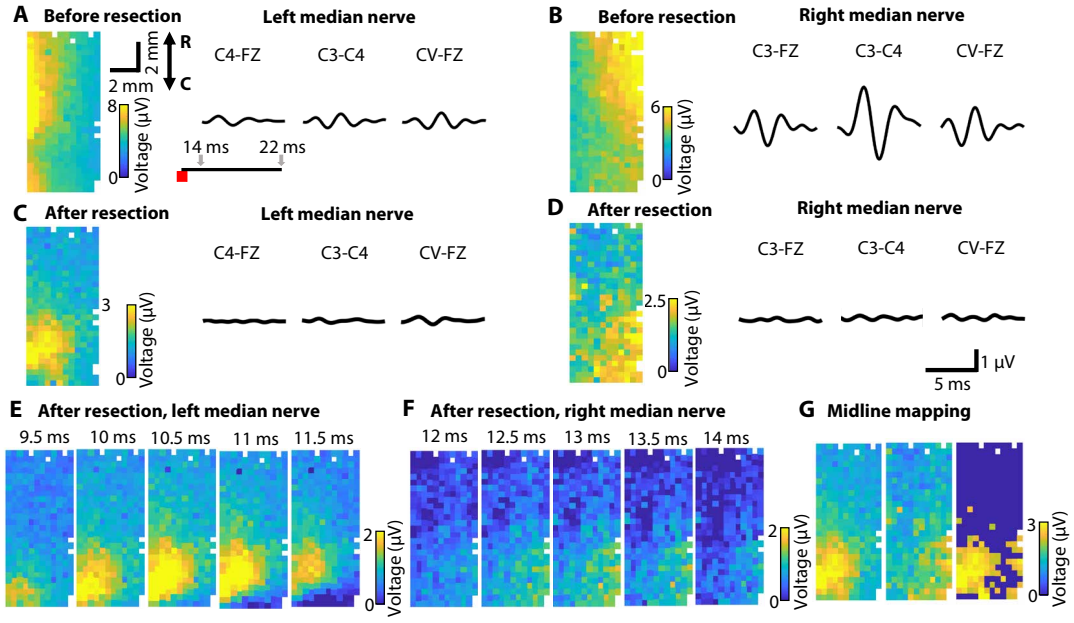

Fig. 5. Comparison to clinical IONM recordings. (**A** to **D**) Subdural preresection and postresection recordings to 30-mA left and right median nerve stimulation. (**E** and **F**) Time evolution of postresection recorded responses to 30-mA left and right median nerve stimulation. (**G**) Functional midline estimation from postresection recorded responses to 30-mA left and right median nerve stimulation.

In this study, we transitioned from PEDOT:PSS to PtNR contacts, which have been shown to be more suitable for stimulation than other low-impedance microelectrode materials (*38*, *39*). Although we do not perform stimulation in this study, having spinal cord electrodes that can both record and stimulate would be the goal for many applications outside of neuromonitoring. The current iteration was a recording electrode only, but a hybrid version of record and stimulate electrode is now under development, where one or a subset of channels delivers the stimulation and the remaining channels record. This, combined with a more robust fabrication process (see Materials and Methods), suggests that PtNR microelectrodes can be a good choice for human neural devices. Our grid was 6 mm wide, as recommended by the surgical team that performed the research in the clinical setting on the first three participants. For two of the last three participants, we were able to identify the midline, and in the third, we could not. Increasing the width of the array and its axial coverage may aid isolation of the midline across diverse participants.

The advantageous design of our research microelectrode allowed us to discriminate stimulation currents at and above 7.5 mA. This is important because 30-mA stimulation, as was used in participant 5, is considered high and may cause a pain response. In general, currents over 10 mA are considered potentially painful (*50*). Therefore, reducing IONM current below this amplitude may benefit the patient by reducing anesthesia interventions during a procedure. However, systematic studies for correlating current amplitudes necessary for capturing when and where neural deficits that occur in dorsal fibers can be formed are yet to be conducted.

Epidural and subdural recordings showed different spatiotemporal features, which means that these placements could offer distinct applications. These differences are important given that epidural placement is easier to achieve and is less invasive. Epidural placement showed peak-to-peak response amplitudes generally on par with subdural placement. However, there was less localization of responses across the array, resulting in an incoherent phase gradient. Surgery that requires identification of the functional midline inherently involves exposure of the dorsal spinal cord and subdural clinical procedures. Therefore, the subdural microelectrode array placement can be a valuable asset for making clinical decisions in such applications because of the high-resolution identification of the functional midline and phase gradients in 2D. On the other hand, although epidural placements cannot resolve spatial variations in the response, they could be informative for evaluating the quality of the response (whether it is present and to what extent), even when IONM responses cannot be detected. This is particularly important for decompression and other surgeries that do not involve opening of the dura mater.

Our research grid was superior compared to the clinical equipment in terms of the sensitivity of the system. We averaged 30 to 40 trials to achieve the mean peak-to-peak amplitude responses at a stimulation rate of 2.78 Hz, therefore requiring 10 to 14 s of recorded data. The clinical equipment stimulates at 1.41 Hz, requires more than 300 trials, and often throws out trials, resulting in a necessary data segment of 4 min or more. This is a large improvement in responsiveness of the system and could allow for quicker detection of neurological damage. In addition, at high current amplitudes, even fewer trials would be necessary with our microelectrode, resulting in practically real-time responsiveness to surgical intervention. In participant 5, we were also able to capture SSEPs with our research microelectrode when the clinical IONM system could not. This participant showed temporary neurological deficit after surgery that quickly improved, which validates that the persistent responses seen by our microelectrode carry clinical value.

There were a few limitations to this study. First, the electrode location varied between participants because surgery was performed at different heights of the cervical spinal cord. This made it

impossible to directly compare recordings between participants. The electrode was also placed in the vicinity of abnormal tumor tissue, which further increased the variability in recordings among patients. In addition, there was slight variation in electrode impedances and the distribution of working channels between electrodes, which introduced more variability in the datasets. Nonetheless, the overall features of the responses were consistent, including response amplitudes, propagation velocity, midline mapping capability, and epidural and subdural recording of spatiotemporal differences. Another limitation of this study was the inability to directly compare the clinical grid recordings and the microelectrode recordings due to different trial numbers used to produce the mean responses. Future studies will need to investigate and quantify these differences more thoroughly. Last, this study included only six patients, with just one patient showing a decrease in SSEP amplitude during surgery. More patients need to be included in future studies to investigate the consistency in the research microelectrode performance and its ability to better detect neurological damage compared to existing IONM equipment.

This study was approved to be performed during operative pauses, and another limitation of this study was the inability to record during the surgical resection, which is a requirement for any IONM system. To address this limitation, we are developing microelectrodes that can surround but still leave access to the resection zone, creating a "window in a grid" that will allow surgical procedures to proceed while providing real-time monitoring of spatiotemporal SSEP patterns from the dorsal surface of the spinal cord. The window-in-a-grid electrode would provide coverage to the rostral and caudal segments of the spinal cord to the surgical plane, thus allowing direct comparison of SSEPs below and above the surgical site. With these improvements in place, our microelectrode system could become a complete and highly detailed IONM system. Furthermore, the PtNR microelectrode grid could be used for more traditional DC mapping given its stimulation capabilities (*37*).

In addition to IONM, we believe that our PtNR microelectrodes have implications for the treatment of SCI by providing a high-resolution, high-coverage spinal cord grid. We speculate that our research grid could potentially be used to capture sensory information from the peripheral nerves below the point of injury to be relayed to the brain, which has been pursued recently (*51*–*53*), and to provide the means for targeted sensory nerve stimulation. For this, further developments will need to be made to capture native sensory pathway neural activity as opposed to recording stimulated SSEPs and to perform stimulation with PtNR electrodes. Last, we also believe that our microelectrode array could mediate SCI treatment by identifying and stimulating the root entry zones in patients with SCI, which has been shown recently to restore motor function (*54*).

In summary, we introduce a high-density microelectrode grid and demonstrate its ability to outperform standard clinical IONM during spinal cord surgery. For both subdural and epidural placements, we evaluated stimulation responses that were present even when IONM did not resolve any responses. Our microelectrode was able to capture detailed spatiotemporal patterns of responses that can define with high precision the 2D maps of the functional midline during surgery. Our use of this grid in high-resolution mapping from the surface of the spinal cord shows that this microelectrode holds the promise for applications that may help neurosurgical procedures and neuromodulation therapies in the spinal cord and beyond.

MATERIALS AND METHODS

Study design

The research objectives of this study were to (i) evaluate whether direct recordings from the human spinal cord could reduce the stimulation thresholds required to detect neurological activity and quantify this difference, (ii) quantify the spatial selectivity of our high–channel count grids and their ability to localize the spinal cord functional midline, (iii) evaluate the differences in epidural versus subdural recordings to determine optimal grid placement, and (iv) assess whether the research grid can identify neurological signal when it is classified as absent by the standard IONM equipment. Randomization was not performed and did not apply to our study because this is a proof-of-concept technology study.

Research grid fabrication, characterization, and sterilization

Both PEDOT:PSS and PtNR research grids were fabricated on 17.78 cm by 17.78 cm by 0.15 cm photomask-grade soda lime glass plate (Nanofilm), which were cleaned via O_2 plasma at 200 W for 5 min. Diluted Micro-90 (0.1%) was spin-coated onto the glass plate to act as a release layer, after which the plate was coated with 3.7-μm-thick parylene C using a parylene deposition system (Specialty Coating Systems 2010 Labcoater). Next, two layers of gold traces (10-nm Cr and 250-nm Au) were deposited onto the plate using standard lithography techniques and AZ5214E-IR photoresist (MicroChemicals). This double layer of leads was found to improve device yield by reducing chance of disconnects due to particles during the photolithography process.

PEDOT:PSS grid fabrication

For PEDOT:PSS grids, the metal traces were then encapsulated in the second and third parylene layers, each 3.1 μm thick. Concentrated Micro-90 [100 μl in 50 ml of deionized (DI) water] was spin-coated before the third parylene coating to allow for peel-off of this layer at a later step. Via (hole) through the parylene was performed via oxygen etching at 200 W for 39 min. PEDOT:PSS solution was spin-coated onto the exposed contacts and cured at 150°C for 60 min, and the third parylene layer was then peeled off. The electrodes were laser cut and lifted off with DI water. Preparation of the PEDOT:PSS solution and more fabrication details can be found in previous publications, including (*39*).

PtNR grid fabrication

PtNR contact formation on parylene C was prepared using a technique previously developed and described in our laboratory (*40*). Briefly, the metal traces and PtAg alloyed contacts were encapsulated in a second 3.1-μm parylene layer. After deposition of a Ti hard mask, the PtAg contacts and connector pads were exposed using a dry etch of the Ti layer with SF_6/Ar gas followed by oxygen dry etching of the paylene C. The samples were lifted off with 6:1 buffered oxide etchant, and the PtAg was dealloyed in 60°C nitric acid for 2 min, thereby forming the PtNRs with Pt/Ag composition of about 95%/5%. The microelectrodes were bonded to custom-made extender printed circuit boards (PCBs) as described in a previous publication (*40*).

The quality of the fabricated devices and their PEDOT:PSS or PtNR contacts were first evaluated using optical microscopy. Impedance magnitude and phase at 1 kHz were then measured to ensure device functionality. If the devices had high yield, then they were sent for sterilization to UCSD's or OHSU's sterilization facility. The sterilization processes used were steam with gravity mode at 121°C for 30 min for PEDOT:PSS electrodes and Sterrad with the default sterilization mode for PtNR electrodes.

Participants and research grid placement

The research participants were patients undergoing an intramedullary spinal cord tumor resection or biopsy procedure at the cervical segment with IONM with both epidural and subdural spinal cord exposure. Participants were recruited by the neurosurgery team involved in this study. All patients voluntarily participated after informed consent in accordance with the University of California IRB. Participants were informed that participating in the study would not affect the treatment they received. Participants could withdraw at any time. Recordings were acquired from six participants.

Surgery proceeded as normal until epidural spinal cord exposure. During the surgical exposure, the recording equipment was set up on the nonsterile side of the OR. The research grid was removed from the sterile tray by a scrubbed-in member of the neurosurgery team. A Situate Sterile Drape (Medtronic 01-0020) was used to interface between the sterile and nonsterile recording elements. The extender board of the research grid was inserted through an opening in the drape and touch-proof connectors of a sterile twisted pair of subdermal needle electrodes were inserted through another hole. Two Tegaderm films (3M) were taped together to seal the openings. A member of the research team then connected the extender board and the recording equipment. The research grid was then placed in sterile saline solution in a kidney dish until the recording started. Impedance was measured to ensure proper equipment connection and grid viability after sterilization. Further details are described in (*40*).

Data collection

Recordings were taken at three time points in the surgery: (i) epidurally after spinal cord exposure; (ii) subdurally, on the pial surface, before tumor resection or biopsy; and (iii) subdurally after tumor resection or biopsy. Impedances were measured and plotted before each recording in both sterile saline and on the spinal cord itself to check for electrode damage and equipment connectivity issues. The total recording time for all three time points did not exceed 30 min during downtime of the surgery, so as not to cause adverse effects to the patient and surgical outcome. Recordings were collected using the Intan RHD Recording Controller at 20-kHz sampling rate. A member of the research team dictated stimulation amplitude and location to the neuromonitoring team member. Notes were taken during stimulation to note approximate stimulation time and amplitude in the recording. Reference and ground needles for the research microelectrode were placed in nearby tissue. The clinical IONM system used to capture data from participants 5 and 6 was Cascade's IOMAX.

Data processing

Research grid data were processed in MATLAB. Data were filtered to remove 60-Hz noise and harmonics using a notch filter. Data were then band-pass–filtered at 30 to 300 Hz. The low frequency was chosen to be 30 Hz to remove changes in voltage due to DC voltage shifts and electrocardiogram artifact, which was below 30 Hz, while preserving the response frequency bandwidth (a spectrogram showed responses in the frequency range of 70 to 150 Hz). Stimulus artifacts from the nonfiltered data were used to determine stimulation time points, and these time points were compared to a custom-made stimulation artifact capture system for initial experiments, but this was found to be redundant for later experiments. Notes taken during surgery were used to classify each stimulus train on the basis of the stimulation amplitude and location. Responses were computed by averaging a 20-ms time window after each stimulus artifact. Baseline data were computed by averaging a 20-ms time window within 20 to 80 ms before stimulus artifact. The onset of the time window varied between stimulations and was chosen to ensure that no aberrant signals were present in the baseline recording. Baseline values were then subtracted from the averaged responses. Peak-to-peak amplitude was calculated by taking the difference between the highest and lowest data points in the time window of 5 to 20 ms after stimulus and within the 20-ms time window for baseline. The clinical data were downloaded from the IONM software IOMAX (Cascade) in the form of a .json file after the case. The data were band-pass–filtered at 30 to 750 Hz. The data were imported and plotted in Python along with corresponding time stamps and event notes from the IONM team.

Midline mapping

An SNR thresholding technique was used to evaluate the functional midline. The mean and SD of the baseline peak-to-peak amplitude was calculated. For both the left- and right-side stimulation, peak-to-peak amplitudes of the response with root mean square numbers less than a certain value were zeroed (Eq. 1), thus creating individual threshold maps for each side. For participant 5, the value of 13 was arbitrarily chosen for the subdural recording based on the number of channels that did not meet this criterion. The value of 18 was chosen for the epidural recording. The left- and right-side threshold maps were combined by taking the square root of the sum of squared thresholds (Eq. 2)

$$\text{find}\left(\frac{\text{intensities} - m}{\text{std}}\right) < \text{val} = 0 \quad (1)$$

$$\sqrt{\text{intensities}_{\text{right}}^2 + \text{intensities}_{\text{left}}^2} = \text{combined intensities} \quad (2)$$

Phase gradient analysis

The spatial phase gradient of the responses was calculated in MATLAB on the basis of previous methods described in literature (*40*, *55*, *56*). The streamlines were generated with the streamline MATLAB function to illustrate the general directional trends of the local spatial phase gradient.

Statistical analysis

We used Welch's test to determine whether there was a significant change in impedance after Sterrad sterilization because we assumed unequal variance between samples. We used the Mann-Whitney *U* test to evaluate statistical significance of the peak-to-peak amplitude responses. This nonparametric test was chosen because the amplitude distributions for each current amplitude deviated slightly from a normal distribution, making a nonparametric test more appropriate. Response peak-to-peak amplitudes were compared against baseline peak-to-peak amplitudes. In each statistical test, the channels in the top 20% based on SNR were used to ensure that the significance was not affected by nonresponsive channels. The *z* score was used to evaluate effect size, which is appropriate for nonparametric data, and multiple test correction was applied to the *P* values because multiple tests were performed to evaluate various current amplitudes and stimulation points. Effect size was calculated by dividing the *z* score by the square root of the number of pairs (Eq. 3). The *z* score was calculated in Python from the *U* statistic (Eq. 4). *P* values were corrected using the Holm method

$$\text{Effect size} = {}^{Z}/_{\sqrt{n}}, \text{where } n = \text{number of pairs} \quad (3)$$

$$Z = \frac{U - {}^{n^2}/_{2} + 0.5}{\sqrt{{}^{n^2*(N+1)}/_{12}}} \quad (4)$$

SUPPLEMENTARY MATERIALS

www.science.org/doi/10.1126/scitranslmed.abq4744
Methods
Figs. S1 to S8
Table S1
Movies S1 to S6
Data file S1

View/request a protocol for this paper from *Bio-protocol*.

REFERENCES AND NOTES

1. P. R. Cooper, Outcome after operative treatment of intramedullary spinal cord tumors in adults: Intermediate and long-term results in 51 patients. *Neurosurg.* **25**, 855–859 (1989).
2. S. H. Chang, Y. G. Park, D. H. Kim, S. Y. Yoon, Monitoring of motor and somatosensory evoked potentials during spine surgery: Intraoperative changes and postoperative outcomes. *Ann. Rehabil. Med.* **40**, 470–480 (2016).
3. Z. Ng, S. Ng, V. Nga, K. Teo, S. Lwin, C. Ning, T. T. Yeo, Intradural spinal tumors—Review of postoperative outcomes comparing intramedullary and extramedullary tumors from a single institution's experience. *World Neurosurg.* **109**, e229–e232 (2018).
4. A. Raco, V. Esposito, J. Lenzi, M. Piccirilli, R. Delfini, G. Cantore, Long-term follow-up of intramedullary spinal cord tumors: A series of 202 cases. *Neurosurg.* **56**, 972–981 (2005).
5. M. K. Tobin, J. R. Geraghty, H. H. Engelhard, A. A. Linninger, A. I. Mehta, Intramedullary spinal cord tumors: A review of current and future treatment strategies. *Neurosurg. Focus* **39**, E14 (2015).
6. T. Verla, J. S. Fridley, A. B. Khan, R. R. Mayer, I. Omeis, Neuromonitoring for intramedullary spinal cord tumor surgery. *World Neurosurg.* **95**, 108–116 (2016).
7. K. Rijs, M. Klimek, M. Scheltens-de Boer, K. Biesheuvel, B. S. Harhangi, Intraoperative neuromonitoring in patients with intramedullary spinal cord tumor: A systematic review, meta-analysis, and case series. *World Neurosurg.* **125**, 498–510.e2 (2019).
8. M. R. Nuwer, E. G. Dawson, L. G. Carlson, L. E. Kanim, J. E. Sherman'jd, Somatosensory evoked potential spinal cord monitoring reduces neurologic deficits after scoliosis surgery: Results of a large multicenter survey. *Electroencephalogr. Clin. Neurophysiol.* **96**, 6–11 (1995).
9. I. E. Sandalcioglu, T. Gasser, S. Asgari, A. Lazorisak, T. Engelhorn, T. Egelhof, D. Stolke, H. Wiedemayer, Functional outcome after surgical treatment of intramedullary spinal cord tumors: Experience with 78 patients. *Spinal Cord* **43**, 34–41 (2005).
10. S.-H. Jin, C. K. Chung, C. H. Kim, Y. D. Choi, G. Kwak, B. E. Kim, Multimodal intraoperative monitoring during intramedullary spinal cord tumor surgery. *Acta Neurochir.* **157**, 2149–2155 (2015).
11. V. Deletis, F. Sala, Intraoperative neurophysiological monitoring of the spinal cord during spinal cord and spine surgery: A review focus on the corticospinal tracts. *Clin. Neurophysiol.* **119**, 248–264 (2008).
12. A. A. Gonzalez, D. Jeyanandarajan, C. Hansen, G. Zada, P. C. Hsieh, Intraoperative neurophysiological monitoring during spine surgery: A review. *Neurosurg. Focus* **27**, E6 (2009).
13. D. B. MacDonald, C. Dong, R. Quatrale, F. Sala, S. Skinner, F. Soto, A. Szelényi, Recommendations of the international society of intraoperative neurophysiology for intraoperative somatosensory evoked potentials. *Clin. Neurophysiol.* **130**, 161–179 (2019).
14. A. R. Møller, S. Ansari, A. A. Cohen-Gadol, Techniques of intraoperative monitoring for spinal cord function: Their past, present, and future directions. *Neurol. Res.* **33**, 363–370 (2011).
15. F. Sala, A. Bricolo, F. Faccioli, P. Lanteri, M. Gerosa, Surgery for intramedullary spinal cord tumors: The role of intraoperative (neurophysiological) monitoring. *Eur. Spine J.* **16**, S130–S139 (2007).
16. E. Weigang, M. Hartert, R. Sircar, P. V. Samson, K. Pitzer, J. Genstorfer, J. Zentner, F. Beyersdorf, Setup of neurophysiological monitoring with tcMEP/SSEP during thoracoabdominal aneurysm repair. *Thorac Cardiovasc Surg.* **53**, 28–32 (2005).
17. H. Singh, R. W. Vogel, R. M. Lober, A. T. Doan, C. I. Matsumoto, T. J. Kenning, J. J. Evans, Intraoperative neurophysiological monitoring for endoscopic endonasal approaches to the skull base: A technical guide. *Scientifica (Cairo)* **2016**, 1751245 (2016).
18. T. Yamada, Somatosensory evoked potentials, in *Encyclopedia of the Neurological Sciences*, M. J. Aminoff, R. B. Daroff Eds. (Academic Press, ed. 2, 2014), pp. 230–238.
19. A. M. Padberg, K. H. Bridwell, Spinal cord monitoring. *Orthop. Clin. North A.* **30**, 407–433 (1999).
20. E. (Enno) Freye, *Cerebral Monitoring in the OR and ICU* (Springer, 2005).
21. Aage Moller, *Intraoperative Neurophysiological Monitoring* (Springer, ed. 3, 2010).
22. A. S. Hilibrand, D. M. Schwartz, V. Sethuraman, A. R. Vaccaro, T. J. Albert, Comparison of transcranial electric motor and somatosensory evoked potential monitoring during cervical spine surgery. *J. Bone Joint Surg. Am.* **86**, 1248–1253 (2004).
23. G. Kimchi, N. Knoller, A. Korn, Y. Eyal-Mazuz, Y. Sapir, A. Peled, R. Harel, Delayed variations in the diagnostic accuracy of intraoperative neuromonitoring in the resection of intramedullary spinal cord tumors. *Neurosurg. Focus* **50**, E21 (2021).
24. R. P. Lesser, P. Raudzens, H. Lüders, M. R. Nuwer, W. D. Goldie, H. H. Morris III, D. S. Dinner, G. K. Reegt, J. F. Hahn, A. G. Shetter, H. H. Ginsburg, A. R. Gurd, Postoperative neurological deficits may occur despite unchanged intraoperative somatosensory evoked potentials. *Ann. Neurol.* **19**, 22–25 (1986).
25. M. O. Kelleher, G. Tan, R. Sarjeant, M. G. Fehlings, Predictive value of intraoperative neurophysiological monitoring during cervical spine surgery: A prospective analysis of 1055 consecutive patients. *J. Neurosurg. Spine* **8**, 215–221 (2008).
26. J. Holsheimer, G. Barolat, J. J. Struijk, J. He, Significance of the spinal cord position in spinal cord stimulation. *Acta Neurochir. Suppl.* **64**, 119–124 (1995).
27. J. Holsheimer, G. Barolat, Spinal geometry and paresthesia coverage in spinal cord stimulation. *Neuromodulation* **1**, 129–136 (1998).
28. A. I. Mehta, C. A. Mohrhaus, A. M. Husain, I. O. Karikari, B. Hughes, T. Hodges, O. Gottfried, C. A. Bagley, Dorsal column mapping for intramedullary spinal cord tumor resection decreases dorsal column dysfunction. *J. Spinal Disord. Tech.* **25**, 205–209 (2012).
29. D. S. Yanni, S. Ulkatan, V. Deletis, I. J. Barrenechea, C. Sen, N. I. Perin, Utility of neurophysiological monitoring using dorsal column mapping in intramedullary spinal cord surgery. *J. Neurosurg. Spine* **12**, 623–628 (2010).
30. V. Deletis, F. Sala, The role of intraoperative neurophysiology in the protection or documentation of surgically induced injury to the spinal cord. *Ann. N. Y. Acad. Sci.* **939**, 137–144 (2001).
31. D. Nair, V. M. Kumaraswamy, D. Braver, R. D. Kilbride, L. F. Borges, M. V. Simon, Dorsal column mapping via phase reversal method: The refined technique and clinical applications. *Neurosurg.* **74**, 437–446 (2014).
32. A. Quinones-Hinojosa, M. Gulati, R. Lyon, N. Gupta, C. Yingling, Spinal cord mapping as an adjunct for resection of intramedullary tumors: Surgical technique with case illustrations. *Neurosurg.* **51**, 1199–1206 (2002).
33. J. Hermiz, L. Hossain, E. M. Arneodo, M. Ganji, N. Rogers, N. Vahidi, E. Halgren, T. Q. Gentner, S. A. Dayeh, V. Gilja, Stimulus driven single unit activity from micro-electrocorticography. *Front Neurosci.* **14**, 55 (2020).
34. J. C. Yang, A. C. Paulk, P. Salami, S. H. Lee, M. Ganji, D. J. Soper, D. Cleary, M. Simon, D. Maus, J. W. Lee, B. V. Nahed, P. S. Jones, D. P. Cahill, G. R. Cosgrove, C. J. Chu, Z. Williams, E. Halgren, S. Dayeh, S. S. Cash, Microscale dynamics of electrophysiological markers of epilepsy. *Clin. Neurophysiol.* **132**, 2916–2931 (2021).
35. M. Ganji, E. Kaestner, J. Hermiz, N. Rogers, A. Tanaka, D. Cleary, S. H. Lee, J. Snider, M. Halgren, G. R. Cosgrove, B. S. Carter, D. Barba, I. Uguz, G. G. Malliaras, S. S. Cash, V. Gilja, E. Halgren, S. A. Dayeh, Development and translation of PEDOT:PSS microelectrodes for intraoperative monitoring. *Adv. Funct. Mater.* **28**, 1700232 (2018).
36. A. C. Paulk, J. C. Yang, D. R. Cleary, D. J. Soper, M. Halgren, A. R. O'Donnell, S. H. Lee, M. Ganji, Y. G. Ro, H. Oh, L. Hossain, J. Lee, Y. Tchoe, N. Rogers, K. Kiliç, S. B. Ryu, S. W. Lee, J. Hermiz, V. Gilja, I. Ulbert, D. Fabó, T. Thesen, W. K. Doyle, O. Devinsky, J. R. Madsen, D. L. Schomer, E. N. Eskandar, J. W. Lee, D. Maus, A. Devor, S. I. Fried, P. S. Jones, B. V. Nahed, S. Ben-Haim, S. K. Bick, R. M. Richardson, A. M. Raslan, D. A. Siler, D. P. Cahill, Z. M. Williams, G. R. Cosgrove, S. A. Dayeh, S. S. Cash, Microscale physiological events on the human cortical surface. *Cereb Cortex* **31**, 3678–3700 (2021).
37. M. Ganji, A. C. Paulk, J. C. Yang, N. W. Vahidi, S. H. Lee, R. Liu, L. Hossain, E. M. Arneodo, M. Thunemann, M. Shigyo, A. Tanaka, S. B. Ryu, S. W. Lee, Y. Tchoe, M. Marsala, A. Devor, D. R. Cleary, J. R. Martin, H. Oh, V. Gilja, T. Q. Gentner, S. I. Fried, E. Halgren, S. S. Cash, S. A. Dayeh, Selective formation of porous Pt nanorods for highly electrochemically efficient neural electrode interfaces. *Nano Lett.* **19**, 6244–6254 (2019).
38. M. Ganji, L. Hossain, A. Tanaka, M. Thunemann, E. Halgren, V. Gilja, A. Devor, S. A. Dayeh, Monolithic and scalable Au nanorod substrates improve PEDOT-metal adhesion and stability in neural electrodes. *Adv. Healthc. Mater.* **7**, e1800923 (2018).
39. M. Ganji, A. Tanaka, V. Gilja, E. Halgren, S. A. Dayeh, Scaling effects on the electrochemical stimulation performance of Au, Pt, and PEDOT:PSS electrocorticography arrays. *Adv. Funct. Mater.* **27**, 1703019 (2017).
40. Y. Tchoe, A. M. Bourhis, D. R. Cleary, B. Stedelin, J. Lee, K. J. Tonsfeldt, E. C. Brown, D. Siler, A. C. Paulk, J. C. Yang, H. Oh, Y. Goo Ro, K. Lee, S. Russman, M. Ganji, I. Galton, S. Ben-Haim, A. M. Raslan, S. A. Dayeh, Human brain mapping with multithousand-channel PtNRGrids resolves spatiotemporal dynamics. *Sci. Transl. Med.* **14**, eabj1441 (2022).
41. R. Vatsyayan, D. Cleary, J. R. Martin, E. Halgren, S. A. Dayeh, Electrochemical safety limits for clinical stimulation investigated using depth and strip electrodes in the pig brain. *J. Neural Eng.* **18**, 046077 (2021).

42. D. B. MacDonald, S. Skinner, J. Shils, C. Yingling; American Society of Neurophysiological Monitoring, Intraoperative motor evoked potential monitoring - A position statement by the american society of neurophysiological monitoring. *Clin. Neurophysiol.* **124**, 2291–2316 (2013).
43. V. Deletis, K. Seidel, Neurophysiological identification of long sensory and motor tracts within the spinal cord, in *Neurophysiology in Neurosurgery* (Elsevier, 2020), pp. 163–175.
44. J. G. McLeod, S. H. Wray, Conduction velocity and fibre diameter of the median and ulnar nerves of the baboon. *J. Neurol. Neurosurg. Psychiatry* **30**, 240–247 (1967).
45. A. Eisen, M. Hoirch, J. White, D. Calne, Sensory group la proximal conduction velocity. *Muscle Nerve* **7**, 636–641 (1984).
46. L. Pelosi, J. B. Cracco, R. Q. Cracco, Conduction characteristics of somatosensory evoked potentials to peroneal, tibial and sural nerve stimulation in man. *Electroencephalogr. Clin. Neurophysiol.* **68**, 287–294 (1987).
47. W. Young, K. Sakatani, Neurophysiological mechanisms of somatosensory-evoked potential changes, in *Neural Monitoring: The Prevention of Intraoperative Injury*, S. K. Salzman, Ed. (Humana Press, 1990), pp. 115–148.
48. J. Isakovic, I. Dobbs-Dixon, D. Chaudhury, D. Mitrecic, Modeling of inhomogeneous electromagnetic fields in the nervous system: a novel paradigm in understanding cell interactions, disease etiology and therapy. *Sci. Rep.* **8**, 12909 (2018).
49. M. J. Kržan, Intraoperative neurophysiological mapping of the spinal cord's dorsal columns, in *Neurophysiology in Neurosurgery*, V. Deletis, J. L. Shils, Eds. (Elsevier, 2002), pp. 153–165.
50. The fatal current. *Phys. Ther.* **46**, 968–969 (1966).
51. K. L. Bunday, M. A. Urbin, M. A. Perez, Potentiating paired corticospinal-motoneuronal plasticity after spinal cord injury. *Brain Stimul.* **11**, 1083–1092 (2018).
52. A. P. Yadav, D. Li, M. A. L. Nicolelis, A brain to spine interface for transferring artificial sensory information. *Sci. Rep.* **10**, 900 (2020).
53. A. P. Yadav, S. Li, M. O. Krucoff, M. A. Lebedev, M. M. Abd-El-Barr, M. A. L. Nicolelis, Generating artificial sensations with spinal cord stimulation in primates and rodents. *Brain Stimul.* **14**, 825–836 (2021).
54. A. Rowald, S. Komi, R. Demesmaeker, E. Baaklini, S. D. Hernandez-Charpak, E. Paoles, H. Montanaro, A. Cassara, F. Becce, B. Lloyd, T. Newton, J. Ravier, N. Kinany, M. D'Ercole, A. Paley, N. Hankov, C. Varescon, L. McCracken, M. Vat, M. Caban, A. Watrin, C. Jacquet, L. Bole-Feysot, C. Harte, H. Lorach, A. Galvez, M. Tschopp, N. Herrmann, M. Wacker, L. Geernaert, I. Fodor, V. Radevich, K. van den Keybus, G. Eberle, E. Pralong, M. Roulet, J.-B. Ledoux, E. Fornari, S. Mandija, L. Mattera, R. Martuzzi, B. Nazarian, S. Benkler, S. Callegari, N. Greiner, B. Fuhrer, M. Froeling, N. Buse, T. Denison, R. Buschman, C. Wende, D. Ganty, J. Bakker, V. Delattre, H. Lambert, K. Minassian, C. A. T. van den Berg, A. Kavounoudias, S. Micera, D. van de Ville, Q. Barraud, E. Kurt, N. Kuster, E. Neufeld, M. Capogrosso, L. Asboth, F. B. Wagner, J. Bloch, G. Courtine, Activity-dependent spinal cord neuromodulation rapidly restores trunk and leg motor functions after complete paralysis. *Nat. Med.* **28**, 260–271 (2022).
55. D. Rubino, K. A. Robbins, N. G. Hatsopoulos, Propagating waves mediate information transfer in the motor cortex. *Nat. Neurosci.* **9**, 1549–1557 (2006).
56. L. Muller, G. Piantoni, D. Koller, S. S. Cash, E. Halgren, T. J. Sejnowski, Rotating waves during human sleep spindles organize global patterns of activity that repeat precisely through the night. *Elife* **5**, e17267 (2016).

Acknowledgments: We acknowledge insightful discussions with T. Yakish and S. H. Lee of UC San Diego. We are grateful for the technical support from the nano3 cleanroom facilities at UC San Diego's Qualcomm Institute where the PtNRGrid fabrication was conducted. This work was performed, in part, at the San Diego Nanotechnology Infrastructure (SDNI) of UC San Diego, a member of the National Nanotechnology Coordinated Infrastructure, which is supported by the National Science Foundation (NSF) (grant ECCS1542148). **Funding:** This work was supported by a 2018 Galvanizing Engineering in Medicine award from the UC San Diego's Altman Clinical and Translational Research Institute to S.A.D., J.D.C., and J.M.; the National Institutes of Health (NIH) award no. NIBIB DP2-EB029757 to S.A.D.; NIH BRAIN Initiative R01NS123655-01 and UG3NS123723-01 to S.A.D.; the NSF award no. 1728497 to S.A.D. and CAREER no. 1351980 to S.A.D.; an NSF Graduate Research Fellowship Program no. DGE-1650112 to A.M.B.; and an NIH F32 MH120886-01 to D.R.C. Any opinions, findings, and conclusions or recommendations expressed in this material are those of the authors and do not necessarily reflect the views of the funding agencies. **Author contributions:** S.A.D., J.D.C., D.R.C., and J.M. conceived the project, which was refined by input from A.M.R. and W.H.A.R.; S.A.D. led all aspects of the project. S.M.R. fabricated the grids, designed the tasks, and conducted all data analysis with S.A.D.'s guidance and with input from Y.T. S.M.R. performed statistical analysis with input from X.Z. S.M.R., D.R.C., A.M.B., B.S., J.M., E.C.B., A.K., W.H.A.R., A.M.R., J.D.C., and S.A.D. performed recordings in the OR. S.A.D. and S.M.R. wrote the manuscript, and all authors discussed the results and contributed to the manuscript writing. **Competing interests:** Y.T., A.M.R., and S.A.D. have equity in Precision Neurotek Inc. that is cofounded by the team to commercialize PtNRGrids for intraoperative mapping. S.A.D. has competing interests not related to this work including equity in FeelTheTouch LLC. S.A.D. was a paid consultant to MaXentric Technologies. D.R.C. has equity in Surgical Simulations LLC. A.M.R. has an equity and is a cofounder of CerebroAI. A.M.R. received consulting fees from Abbott Inc. and Biotronik Inc. **Data and materials availability:** All data associated with this study are present in the paper or the Supplementary Materials. The human spinal recording data can be accessed in Data Archive BRAIN Initiative (DABI) (https://dabi.loni.usc.edu/). Custom Matlab codes (version R2021a) in combination with open-source automatic IID detection (www.ieeg.org) and propagating-wave (https://mullerlab.github.io/) codes were used for the analyses and are available in GitHub (https://srussman.github.io/).

Submitted 11 April 2022
Accepted 12 August 2022
Published 28 September 2022
10.1126/scitranslmed.abq4744

Science Translational Medicine

Constructing 2D maps of human spinal cord activity and isolating the functional midline with high-density microelectrode arrays

Samantha M. RussmanDaniel R. ClearyYoungbin TchoeAndrew M. BourhisBrittany StedelinJoel MartinErik C. BrownXinlian ZhangAaron KawamotoWon Hyung A. RyuAhmed M. RaslanJoseph D. CiacciShadi A. Dayeh

Sci. Transl. Med., 14 (664), eabq4744. • DOI: 10.1126/scitranslmed.abq4744

A roadmap of the spine

During spinal cord surgery, intraoperative neuromonitoring (IONM) is used to reduce the risk of damage. Electrodes on muscles or scalp record the response to large-amplitude electrical stimuli delivered to the spinal cord. However, this method does not allow precise spatiotemporal characterization of spinal cord neurophysiology. Now, Russman *et al.* developed a microelectrode array that can be placed on the spinal cord during surgery and record with high spatiotemporal definition and high sensitivity the electrophysiological response to low-current stimulation, providing precise maps of spinal cord electrophysiology. These maps can be used during surgery to improve IONM.

Science Translational Medicine (ISSN) is published by the American Association for the Advancement of Science. 1200 New York Avenue NW, Washington, DC 20005. The title *Science Translational Medicine* is a registered trademark of AAAS.

Science Translational Medicine
AAAS

Supplementary Materials for

Constructing 2D maps of human spinal cord activity and isolating the functional midline with high-density microelectrode arrays

Samantha M. Russman *et al.*

Corresponding author: Shadi A. Dayeh, sdayeh@eng.ucsd.edu

Sci. Transl. Med. **14**, eabq4744 (2022)
DOI: 10.1126/scitranslmed.abq4744

The PDF file includes:

Other Supplementary Material for this manuscript includes the following:

Supplementary Methods

Case details

Subject 1 was implanted with a 128-channel PEDOT:PSS microelectrode with 300 μm horizontal and 4 mm vertical pitch and with 30 μm diameter contacts. Subject 2 was implanted with a PEDOT:PSS microelectrode grid with 32x16 channels, 1 mm horizontal and 1 mm vertical pitch and 30 μm contact diameter. Subject 3 was implanted with a PEDOT:PSS microelectrode grid with 5x200 channels, 200 μm horizontal and vertical pitch and 90 μm contact diameter. A summary of participants and experimental details are shown in Table S1.

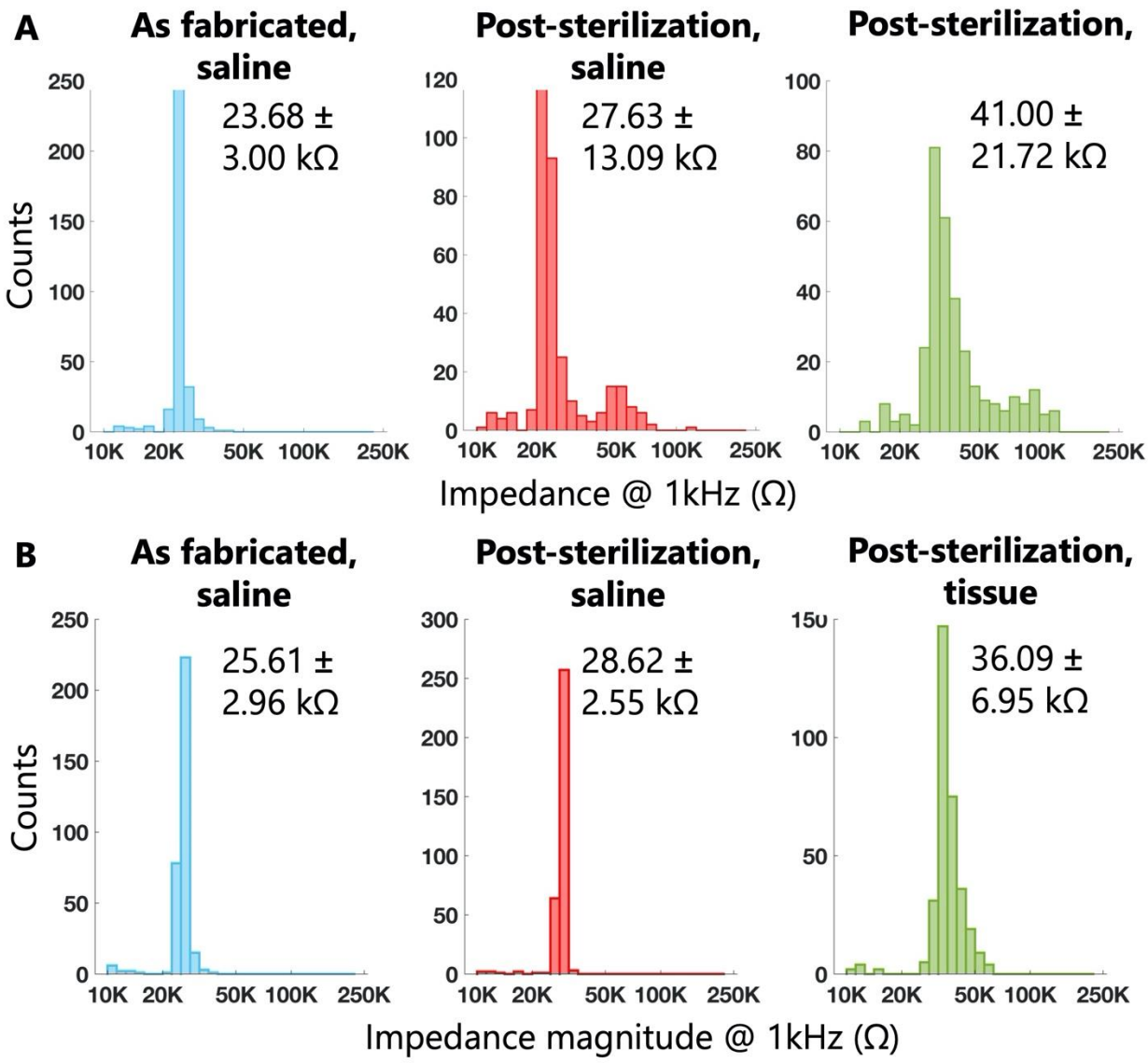

Figure S1. Microelectrode array impedance histograms. 1-kHz impedance magnitude histograms measured as fabricated in saline, post-sterilization in saline, and on spinal cord tissue for (A) subject 4 and (B) subject 6.

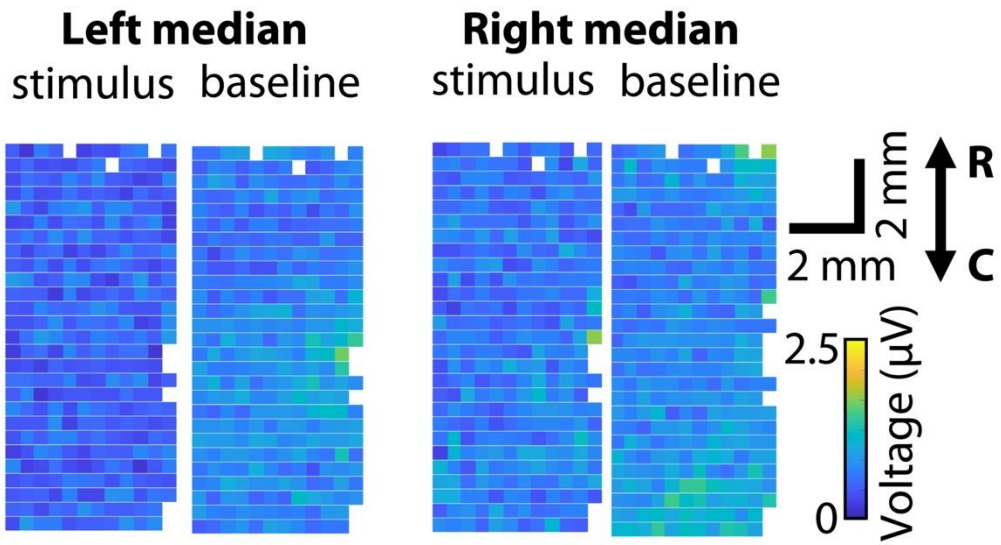

Figure S2. Skin control recordings during 30 mA left and right median nerve stimulation for subject 5.

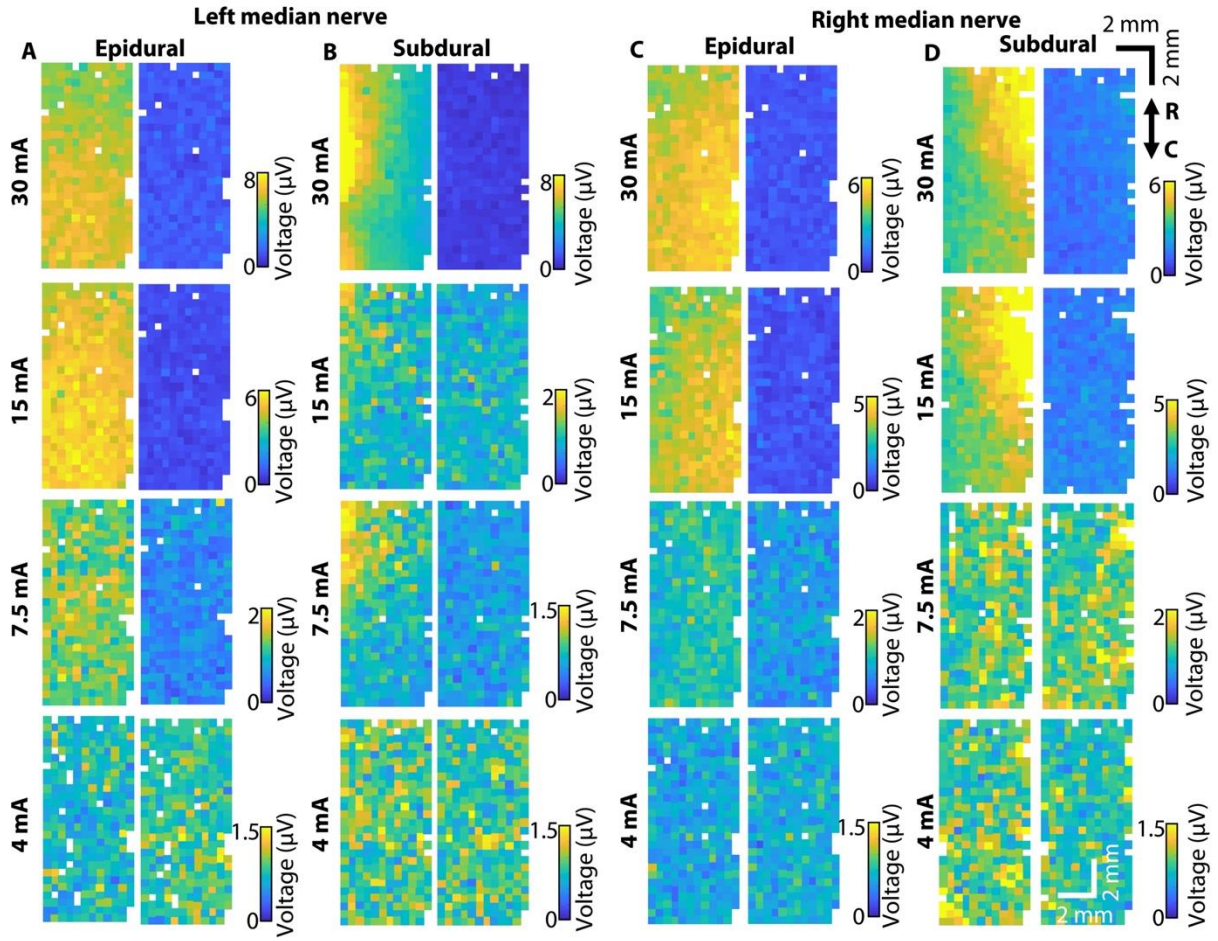

Figure S3. Peak-to-peak amplitude responses from subject 5. (A) – (D) Spatial distribution of peak-to-peak amplitudes of responses to both left and right median nerve stimulation recorded epidurally and subdurally pre-resection. Left panels show the response peak-to-peak amplitudes. Right panels show the baseline peak-to-peak amplitudes. Peak-to-peak amplitudes were calculated from the time evolution plots of Fig. 2 as described in Methods.

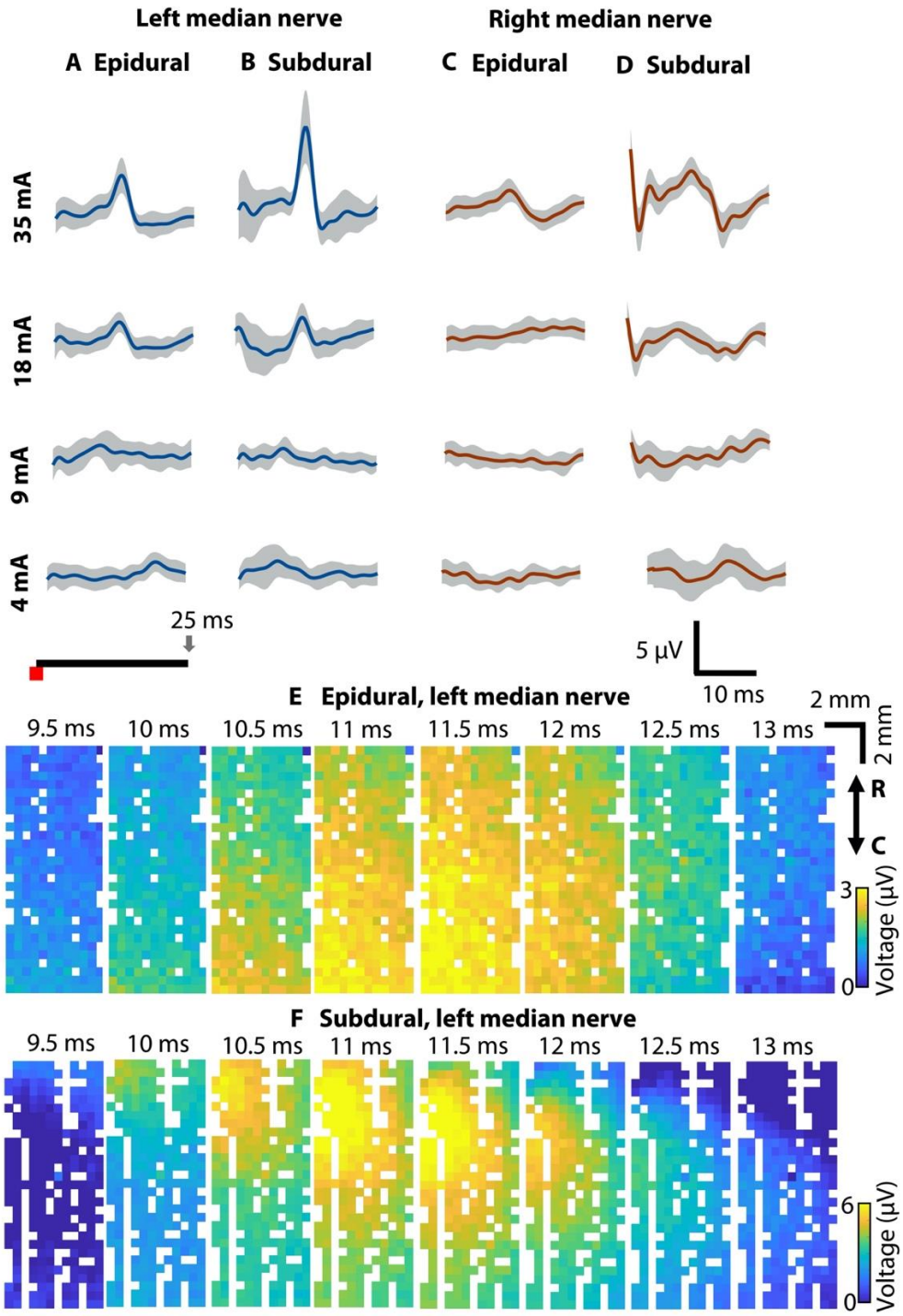

Figure S4. Single channel response and time evolution plots from subject 4. (A) – (D) Maximal single channel responses to left and right median nerve stimulation in both epidural and subdural placements. (E) Epidurally and (F) subdurally recorded time evolution of responses to left median nerve stimulation.

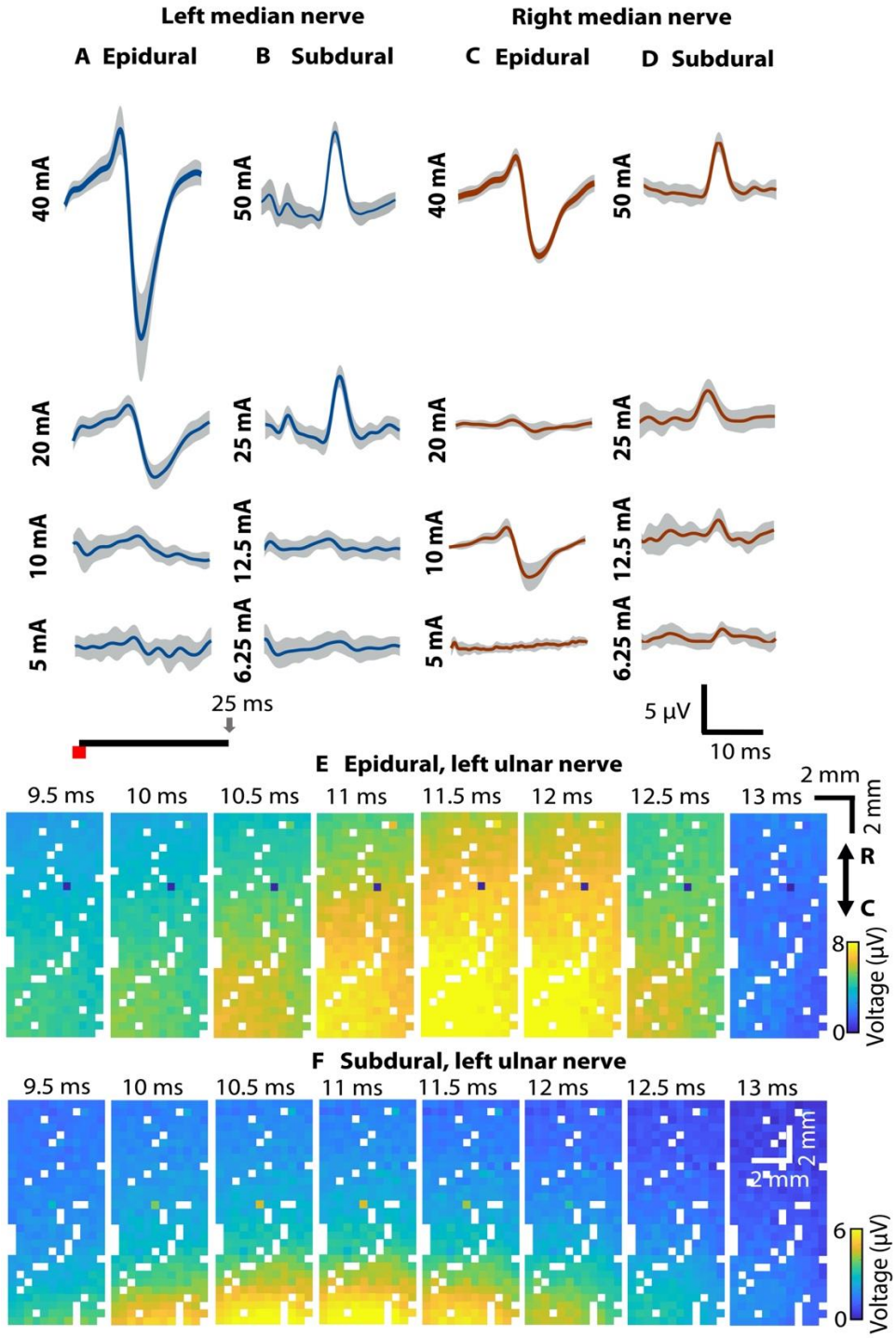

Figure S5. Single channel response and time evolution plots from subject 6. (A) – (D) Maximal single channel responses to left and right ulnar nerve stimulation in both epidural and subdural placements. In this subject, the spinal cord was heavily displaced to the right due to the tumor (see Table S1) and the localization of SSEPs on the electrode array was likely impacted by this displacement. (E) Epidurally and (F) subdurally recorded time evolution of responses to left ulnar nerve stimulation.

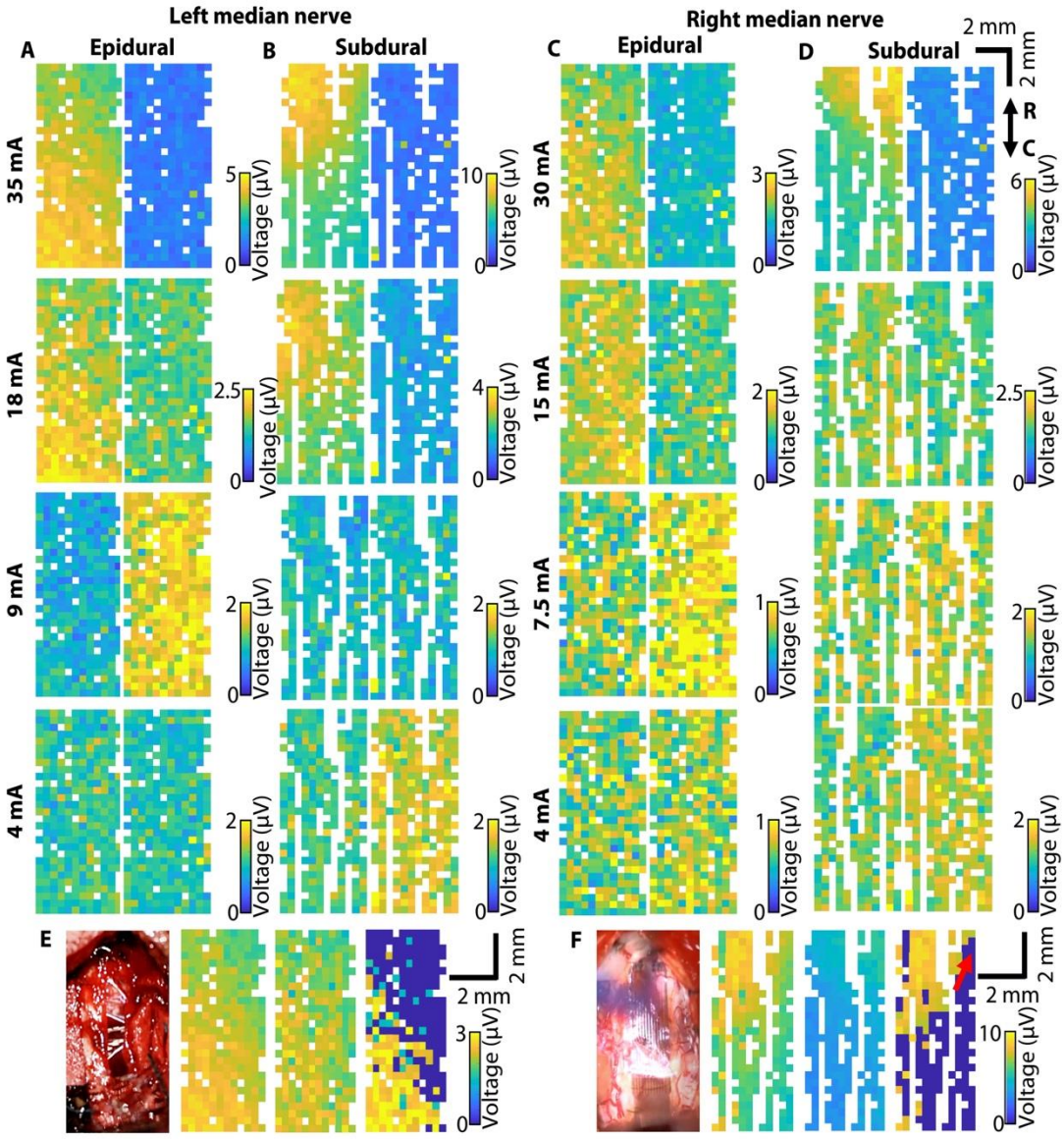

Figure S6. Peak-to-peak amplitude responses from subject 4. (A) – (D) Spatial distribution of peak-to-peak amplitudes of responses to both left and right median nerve stimulation recorded epidurally and subdurally pre-resection. Left panels show the response peak-to-peak amplitudes. Right panels show the baseline peak-to-peak amplitudes. (E) Functional midline estimation from epidural recording of responses to 30 mA left and right median nerve stimulation. (F) Functional midline estimation from subdural recording of responses to 30 mA left and right median nerve stimulation.

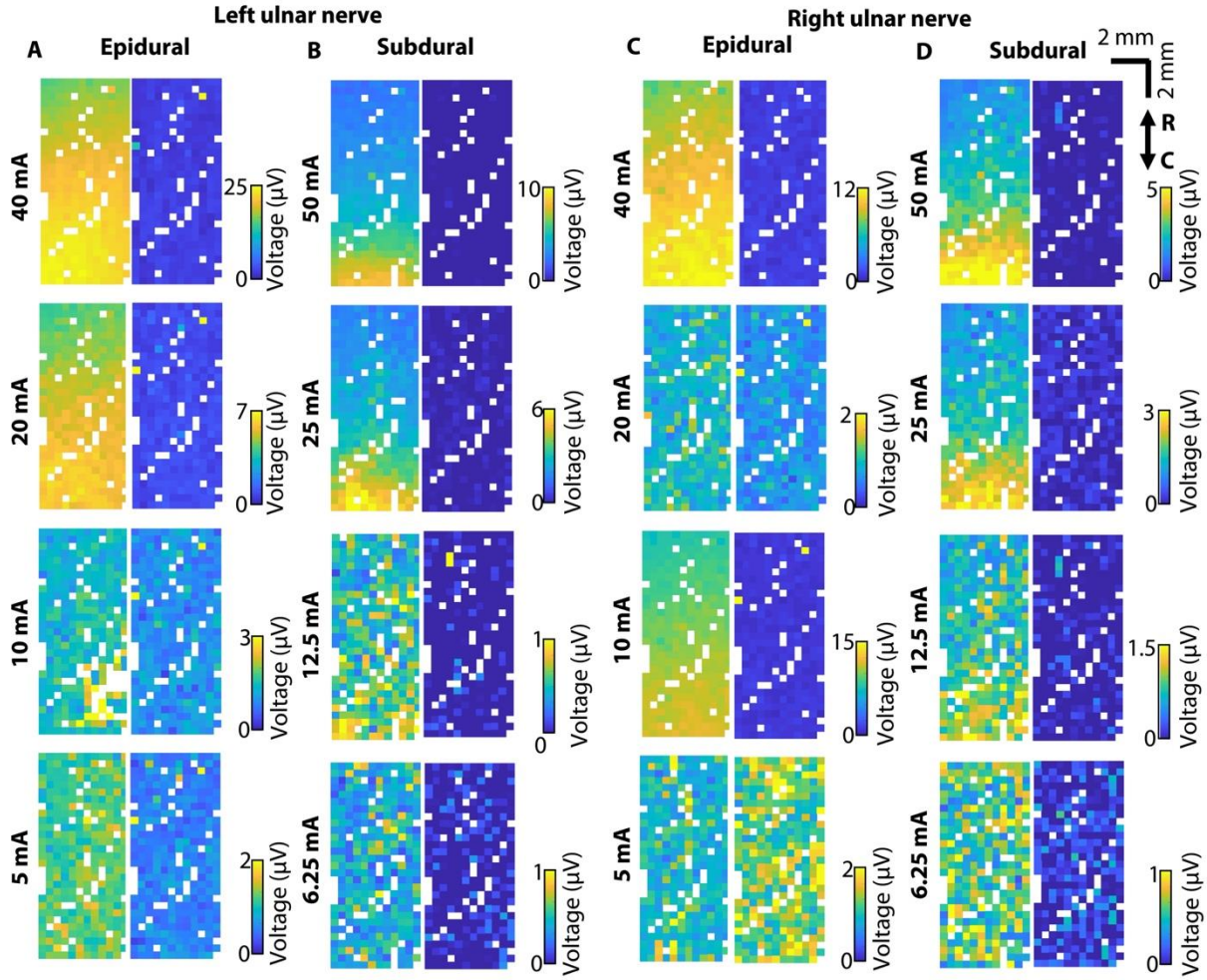

Figure S7. Peak-to-peak amplitude heatmaps from subject 6. (A) – (D) Spatial distribution of peak-to-peak amplitudes of responses to both left and right ulnar nerve stimulation recorded epidurally and subdurally post-resection. Left panels show the response peak-to-peak amplitudes. Right panels show the baseline peak-to-peak amplitudes. In this subject, the tumor displaced the spinal cord severely to the right and the electrode array was placed over the left dorsal column. Responses to left ulnar nerve stimulation were 2x greater in amplitude compared to right ulnar nerve stimulation.

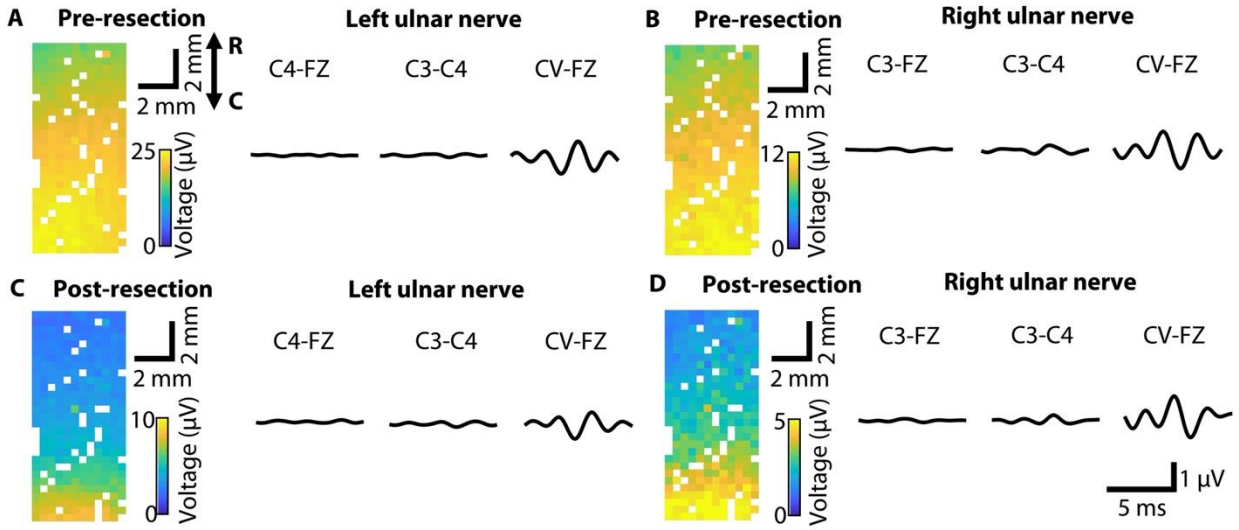

Figure S8. Comparison to clinical IONM recordings in subject 6. (A) – (D) Epidural pre-resection and subdural post-resection recordings to left and right 30 mA median nerve stimulation.

Table S1. Summary of performed cases.

Participant #	Spinal segment	Pre-op deficits	SSEP stimulation	Electrode
1	L1	No deficits	Median nerve	PEDOT:PSS, 4x32, d = 30 µm
2	C2-C5	Weakness in both arms and legs, worse on right side	Median nerve	PEDOT:PSS, 16x32, d=30 µm
3	C2-C5	No deficits	Median nerve	PEDOT:PSS, 5x200, d=30 µm
4	C5-C6	Weakness in left arm and leg	Median nerve	PtNR, 12x31, d=30 µm + multidiam array
5	C4-C5	Mild weakness on both sides of the body, upper SSEPs absent during resection	Median nerve	PtNR, 12x31, d=30 µm + multidiam array
6	C3-C6	Mild weakness in both hands, spinal cord pushed to right	Ulnar nerve	PtNR, 12x31, d=30 µm + multidiam array

Movie S1. Time evolution of the epidurally recorded SSEP phase gradients and streamlines to 30 mA left median nerve stimulation.

Movie S2. Time evolution of the epidurally recorded SSEP phase gradients and streamlines to 30 mA right median nerve stimulation.

Movie S3. Time evolution of the pre-resection subdurally recorded SSEP phase gradients and streamlines to 30 mA left median nerve stimulation.

Movie S4. Time evolution of the pre-resection subdurally recorded SSEP phase gradients and streamlines to 30 mA right median nerve stimulation.

Movie S5. Time evolution of the post-resection subdurally recorded SSEP phase gradients and streamlines to 30 mA left median nerve stimulation.

Movie S6. Time evolution of the post-resection subdurally recorded SSEP phase gradients and streamlines to 30 mA right median nerve stimulation.

Datafile S1: Raw data (provided as separate Excel file)